Please fill in the name of the event you are preparing this manuscript for.	SPE Europec featured at 82nd EAGE Conference and Exhibition
Please fill in your 6-digit SPE manuscript number.	SPE-200593-MS
Please fill in your manuscript title.	Early and Late Time Analytical Solutions for Co-current Spontaneous Imbibition and Generalized Scaling

Please fill in your author name(s) and company affiliation.

Given Name	Middle Name	Surname	Company
Pål	Østebø	Andersen	1 Department of Energy Resources, University of Stavanger, 4036 Norway 2 The National IOR Centre of Norway, University of Stavanger, 4036 Norway

Abstract

We propose an explicit analytical solution for 1D co-current spontaneous imbibition where a core is exposed to water (inlet) and oil (outlet). The system is described using (1) an advection-capillary diffusion transport equation combined with (2) a pressure equation. By ignoring the capillary diffusion term in the transport equation the analytical solution follows in terms of Buckley-Leverett (BL) saturation profiles. The capillary force appears in the pressure equation and determines the advective term of the transport equation. The time when the front reaches the outlet (critical time) is calculated and used for scaling. The solution is extended to after critical time (late time) by maintaining the BL profile inside the system, thus preserving continuity in recovery and spatial profiles. The solution is characterized by an effective total mobility and capillary pressure (incorporating the entire saturation functions), both constant at early time (before critical time). At late times they change dynamically. The model states that imbibition rate can increase, decrease and stay constant with time based on a new mobility ratio being less than, more than or equal to 1, respectively. The ratio also indicates effectiveness of oil displacement. Square root of time recovery is a special case only seen for (very) favorable mobility ratio. The model predicts that co-current imbibition scales with the square of length both at early and late times and that the solution can scale saturation functions.

The analytical solution was compared against numerical simulations of the full system. The new mobility ratio reflected the evolution in co-current recovery better than total recovery. The analytical solution showed too high imbibition rate at favorable mobility ratio. The diffusion term is important then due to strong saturation gradients and the resulting smoothened profile yields lower imbibition rate from the pressure equation. The analytical solution showed too low imbibition rate at early times for unfavorable mobility ratio due to not accounting for rapid early counter-current production. The analytical

solution predicted too high imbibition rate at late times because the BL profile does not capture the oil mobility restriction at the outlet at late times. The time of water reaching the outlet was underestimated by a factor ~2 for strongly water-wet simulations and ~10 for mixed-wet simulations. Scaling recovery with length squared was exact for all times. Scaling recovery until water reaching the outlet demonstrated consistency across saturation functions and viscosities. The analytical solution could match literature experimental data and produce corresponding saturation functions.

To our knowledge, previous analytical solutions have only considered infinite-acting systems (early time), assumed piston-like displacement (uniform saturations on both sides of a saturation shock front) or are implicit, thus not providing more insight than numerical simulations.

Keywords: Co-current spontaneous imbibition; Scaling of recovery factor; Viscosity ratio; Capillary forces

Nomenclature

Roman

f_w	=	Water fractional flow function, -
J	=	Scaled capillary pressure, -
K	=	Absolute permeability, m^2
k_{ri}	=	Relative permeability, -
L	=	System length, m
n_i	=	Corey exponent, -
P_c	=	Capillary pressure, Pa
P_{cbo}	=	Capillary back pressure to oil at the inlet, Pa
p_i	=	Phase pressure, Pa
p_{iL}, p_{iR}	=	Phase pressure at left and right boundary, Pa
$q_a,\ q_b, q_c, r_a, r_b$	=	J-function parameters, -
RF^{co}	=	Outlet produced recovery factor of obtainable oil by spontaneous imbibition, -
RF^{cou}	=	Inlet produced recovery factor of obtainable oil by spontaneous imbibition, -
RF	=	Recovery factor of obtainable oil by spontaneous imbibition, -
s_{eq}	=	Water saturation where capillary pressure is zero, -
s_f	=	Front water saturation, -
s_i	=	Phase saturation, -
s_{ir}	=	Critical phase saturation, -
s_{wR}	=	Water saturation at the right system boundary, -
$\bar{s}_w$	=	Average water saturation, -
S_w	=	Normalized water saturation, -
t	=	Simulation time, s
t_c	=	Critical time when the water front reaches the outlet, s
u_i	=	Darcy phase velocity, m/s
x_f	=	Front position, m

Greek

$\Delta J^*, \Delta J^{**}$	=	Reduction of scaled capillary pressure driving force due to saturation profile (early and late times), -
λ_i	=	Phase mobility, 1 / (Pa s)
$\lambda_T^*, \lambda_T^{**}$	=	Effective total mobility of the saturation profile behind the front (early and late times), 1 / (Pa s)
μ_i	=	Phase viscosity, Pa s
ϕ	=	Porosity, -

Indices

c	=	Capillary
i	=	Phase
o	=	Oil
T	=	Total
w	=	Water

Abbreviations

BL	=	Buckley-Leverett
COC	=	Co-current
COUC	=	Counter-current
MW	=	Mixed-wet
PLD	=	Piston-like displacement
SI	=	Spontaneous imbibition
SWW	=	Strongly water-wet

1. Introduction

Capillary forces play an important role in porous media. They influence initial reservoir fluid distributions (Leverett 1941; Pickell et al. 1966; Vavra et al. 1992), trapping and storage of carbon dioxide (Chiquet et al. 2007, Berg and Ott 2012; Al-Menhali et al. 2015; Krevor et al. 2015), water holdup and resulting production blockage following hydraulic fracturing in unconventionals (Roychaudhuri et al. 2014; Meng et al. 2015; Shen et al. 2016; Zhou et al. 2016) and capillary end effects in core flooding (Leverett 1941; Reed and Maas 2018; Andersen et al. 2020). Spontaneous imbibition (SI), is the focus of this work, and describes spontaneous uptake of wetting fluid (here termed water) into a porous medium due to capillary forces and the simultaneous displacement of non-wetting fluid (here termed oil) (Mason and Morrow 2013). This process is important for recovery of oil and gas in naturally fractured reservoirs where hydrocarbons are stored in disconnected matrix blocks. SI is driven by capillary pressure gradients and water travels towards higher capillary pressures. This causes capillary pressure to decrease towards zero, corresponding to infinite radius of curvature in the surroundings. At this state SI stops. Wettability alteration chemicals in the imbibing fluid (e.g. surfactants, ketone, smart water) can however advance the SI process (Zhang et al. 2006; Fathi et al. 2011; Karimi et al. 2016; Alvarez and Schechter 2017; Wang et al. 2019).

Fluid displacement during SI depends on boundary conditions. If the system is symmetric, e.g. exposed to water on all sides, or is 1D with only one face open the flow tends to be counter-current (COUC) with oil flowing in opposite direction of water. The majority of lab experiments on SI tend to apply the all faces open setup, termed the Amott test (Amott 1959), since it does not involve special treatment of the core boundaries (Hamon and Vidal 1986; Xie and Morrow 2001) and since more faces open reduce the time to conduct the test (Mattax and Kyte 1962; Standnes 2004; Ma et al. 1997). When the system is not symmetric, with wetting phase exposed to some core surfaces and nonwetting phase exposed to others simultaneously, a different flow pattern emerges. In a 1D system with water on one side (termed inlet side) and oil on the other side (termed outlet) most of the produced oil will leave at the outlet (co-current production) and only some at the inlet (counter-current production), although all the water necessarily only can enter from the inlet (Hamon and Vidal 1986). A net co-current flow from inlet towards the outlet occurs. This flow mode is very important since all matrix blocks will be partly covered by water and oil at the beginning of water injection or production from strong aquifer drive reservoirs and since this production mode is more efficient than counter-current production (Pooladi-Darvish and Firoozabadi 2000). Hence, a great deal of production can take place before the blocks are fully submerged in water and fully counter-current production takes place.

The majority of experimental and modelling works on co-current (COC) SI appears to fall in two

categories. In the first the tests are 1D with a core exposed to different phases on opposite ends (Haugen et al. 2014, 2015; Meng et al. 2017). In the other a core / matrix block, or a stack of such are initially surrounded by nonwetting phase and then exposed to a rising or constant water level (Terez and Firoozabadi 1999; Pooladi-Darvish and Firoozabadi 2000; Hamidpour et al. 2015; Meng et al. 2019). This is a 2D/3D configuration where the changing boundary conditions with time and multiple surfaces give rise to more complex flow patterns than the 1D cases. Our focus and further review are limited to the 1D setup.

The extent of counter-current production during COC SI depends on mobility ratio. At favorable mobility ratios where the wetting phase was varied Haugen et al. (2014) and Meng et al. (2016) observed negligible counter-current production, while at unfavorable mobility ratio where the non-wetting phase viscosity was varied, Haugen et al. (2015) and Meng et al. (2017) observed more significant counter-current production. Further, several works (Bourbiaux and Kalaydjian 1990; Standnes et al. 2017; Standnes and Andersen 2017; Andersen et al. 2019c, 2020a) have investigated that lower effective relative permeabilities can be encountered during counter-current flow compared to co-current flow. That can be explained using a generalization of Darcy's law stating that the flux u_i of a phase i is not only proportional to its pressure gradient $\partial_x p_i$, but also to the other flowing phase's pressure gradient. E.g., for water $u_w = -\lambda_{ww}\partial_x p_w - \lambda_{wo}\partial_x p_o$ (and similar for oil), where λ_{ww} and λ_{wo} are generalized mobilities. Andersen et al. (2019c) demonstrated that this effect (viscous coupling) shifted more of the counter-current production to co-current. Non-equilibrium effects have been explored in porous media flow settings (Silin and Patzek 2004; Le Guen and Kovscek 2006; Wang et al. 2018), but to our knowledge not for COC SI. Lenormand et al. (1988), Zhang et al. (2011) and Liu et al. (2015) demonstrated the importance of phenomena at the pore scale and characterized forced displacement of wetting fluid in micromodels into capillary fingering, viscous fingering and stable displacement where respectively; clusters of undisplaced pores were left surrounded according to the path of least capillary resistance; a few established flow paths fingered directly towards the outlet; or the pores were similarly well displaced giving high end recovery. Such behavior can mainly be captured using heterogeneous 2D models and will not appear with standard modeling approaches. Several authors have mentioned the importance of capillary back pressure during SI (Li et al. 2006; Unsal et al. 2007; Haugen et al. 2014, 2015; Andersen et al. 2019c). This is an added resistance for oil to enter the external water phase as droplets compared to being produced into oil as a continuous phase. Hence, if it is nonzero, the driving force for counter-current production will be reduced. This parameter can reduce imbibition rate during COUC SI and can be estimated from the level of counter-current production in experimental data during COC SI.

Analytical solutions have been suggested for COC SI in the past, mainly for strongly water-wet media. The assumption of piston-like displacement (PLD) has often been applied, i.e. where two uniform saturations are separated by a moving front. Some of the earliest work on COC SI was by Washburn (1921) who investigated capillary rise of liquids displacing air in capillary tubes. By use of Poiseuille's law and Young's law to estimate the capillary driving force and neglecting gravity they showed that imbibed volume increases proportionally with the square root of time. Li and Horne (2001) assumed water displaced gas in PLD manner during SI and that gas had infinite mobility, but accounted for gravity. They derived an expression to calculate capillary pressure and water relative permeability at the front from a linear plot of experimental data. They later used the model to scale experimental water-gas data (Li and Horne 2004). Li (2007) used the PLD approach of the mentioned works extended to water-oil tests and predicted a square root of time recovery solution for COUC SI and COC SI based on mobilities and capillary pressure of both phases evaluated at the front saturation. However, they only validated the solution against experimental COUC SI data. Bourbiaux (2009) derived a PLD model that accounted for gravity, capillary forces and mobility ratio and expressed time as function of front position. Haugen et al. (2014) and Fernø et al. (2015), considered capillary forces only and COC SI in an experimental setting where the relative front position with time was shown to be of the form $\sqrt{D^2 + Et} - D$ for parameters D, E. Determining these parameters from regression of experimental data allowed estimation of mobility ratio and the front capillary pressure. They also showed that in situ measurement of pressure (behind the water front) would determine the capillary back pressure as the pressure when counter-current production

ceases. Andersen et al. (2019a) added the effect of a low permeable inlet filter to the COC SI setup and analytical model and demonstrated that linear recovery with time would be obtained regardless of viscosity ratio if this filter was dominating. Previous solutions had demonstrated that imbibition rate could increase with time for unfavorable mobility ratio and decline with favorable mobility ratio which was reproduced as a special case.

Andersen et al. (2019a) interpreted, by means of full numerical simulation, a vast set of own experimental data and data from Meng et al. (2017) where non-wetting phase viscosity was changed systematically. It was shown that PLD is only reasonable when the mobility ratio is favorable, while a smoothened Buckley-Leverett (BL) profile is a close approximation both for that case and unfavorable mobility ratios. Important conclusions were also that imbibition rate falls drastically when the water reaches the outlet. For unfavorable mobility ratio this can give the impression of a low residual oil saturation, although it was seen only to be related to a mobility restriction at the outlet trapping the mobile oil centrally in the core.

Generalized analytical solutions for COUC SI and COC SI were presented by McWhorter and Sunada (1990) in integral form. Their solution accounted for arbitrary relative permeability and capillary pressure functions and they showed that the solution for saturation profile $x(s_w)$ could be written as $x(s_w) = G'(s_w)t^{0.5}$ where G is a function of saturation differing for the two setups. The co-current system solution was limited by the assumption of water influx only and no opposite flux of oil at the inlet which does not allow counter-current production. The counter-current system solution assumed opposite flux boundary condition. Both assumed infinite system length and an inlet water flux boundary condition given by a constant divided by the root of time, where the constant could be determined. Schmid and Geiger (2011) showed that this flux boundary condition was consistent with the counter-current setup. However, this boundary condition directly implies a recovery profile proportional with the square root of time which is seen for COUC SI at early times, but not always for COC SI systems, where imbibition rate both can be constant, decrease or increase with time (Haugen et al. 2014, 2015; Meng et al. 2016, 2017; Andersen et al. 2019a). Hamidpour et al. (2015), reported COC SI tests with oil-to-water viscosity ratios between 0.9 and 16. They fitted recovery for all tests to be proportional to the square root of time, but did not require recovery to start at zero. It will be demonstrated in this work that recovery proportional to square root of time is reasonable for COC SI only when the non-wetting phase mobility is high compared to that of the wetting phase. Deng and King (2019) constructed a semi-analytical solution for COC SI using a Lagrangian approach. An effective fractional flow function dependent on both time and saturation was updated continuously. Although their solution accounted for more general inlet boundary conditions than previous solutions, the final equations were highly coupled differential equations that needed to be solved iteratively and at each time step some values needed be determined in order to maintain correct boundary conditions. The solution was valid only until water reached the outlet.

The COC SI problem consists of solving an advection-diffusion equation where both terms are driven by capillary pressure and the advection term is determined by solving a pressure equation. The interested reader may also consider works where the advective term has been given a forced imbibition component (a set injection rate). Yortsos and Fokas (1983) defined specific saturation function forms that allowed explicit analytical solutions with the BL solution as a special case. The mobility ratio and the ratio of advective to capillary forces could be varied. Wang and Sheng (2018) derived a self-similar solution for forced and spontaneous imbibition under the condition that injection rate was inversely proportional to the square root of time. An effective fractional flow function depending on the injection rate was derived giving a solution similar in form to that of McWhorter and Sunada (1990).

It appears that most or all solutions for COC SI are limited by assumptions of piston-like displacement, strongly water-wet system, infinite-acting systems (do not account for the time after the outlet is reached), are in integral form, apply unreasonable boundary conditions (such as imposing how imbibition rate changes with time) or are non-transparent. The aim of this work is to address these limitations by deriving explicit analytical solutions for COC SI for both strongly and mixed wetting states, for arbitrary saturation functions, that represent times before and after the water has reached the outlet. A general time scale is presented for scaling imbibition data relative to the time when the outlet front is

reached.

We present general equations for COC SI, main assumptions and description of the analytical solution in **Section 2**. The full derivation is found in **Appendices A**, **B** and **C**. Simulation results and comparison to numerical solutions of the general system and experimental data are shown in **Section 3**. The paper is concluded in **Section 4**.

2. Theory

A 1D horizontal core is considered, open for flow from two sides; at $x = 0$ (inlet) and $x = L$ (outlet). The setup is presented in **Figure 1**, where the x-axis is aligned along the core. The core is exposed to water at the inlet and oil at the outlet. COC SI of water at the inlet occurs provided positive capillary pressure exists, i.e. the core is mixed-wet or strongly water-wet. Co-current oil production occurs at the outlet while counter-current production occurs at the inlet. The phases water (w) and oil (o) are described by their saturations s_i and pressures p_i (i=w, o). The core is assumed homogenous regarding porosity ϕ, permeability K and wettability and these properties are not changing with time. The rock and fluids are incompressible and immiscible.

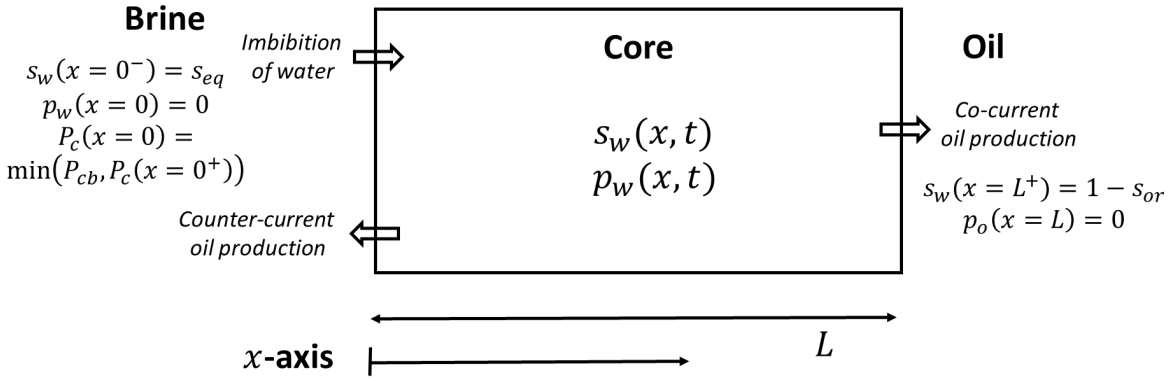

Figure 1 Setup for the co-current spontaneous imbibition system with important boundary conditions and parameters indicated.

2.1. Model for co-current spontaneous imbibition accounting for capillary back pressure

Mass balance equations consistent with the above assumptions are given by (Chen et al. 2006):

$$\phi \partial_t s_w = -u_T \partial_x f_w - K \partial_x (\lambda_o f_w \partial_x P_c), \tag{1}$$

$$\partial_x u_T = 0, \tag{2}$$

$$u_T = u_w + u_o = -K(\lambda_o \partial_x P_c + \lambda_T \partial_x p_w), \tag{3}$$

where the following terminology has been applied:

$$\lambda_T = \lambda_o + \lambda_w, \qquad f_w = \frac{\lambda_w}{\lambda_T}, \qquad \lambda_i = \frac{k_{ri}}{\mu_i}, \qquad (i = o, w) \tag{4}$$

u_T is the total Darcy velocity, f_w water fractional flow function, λ_i phase mobilities defined by the ratio of relative permeability k_{ri} and viscosity μ_i. P_c is the imbibition capillary pressure function, defined as the difference between oil and water pressures. It can be scaled to obtain the dimensionless Leverett J-function (Dullien 2012, Bear 2013):

$$P_c(s_w) = p_o - p_w, \qquad J(s_w) = \frac{P_c}{\sigma_{ow}} \sqrt{\frac{K}{\phi}} \tag{5}$$

where σ_{ow} is the oil-water interfacial tension. The core initially has critical water saturation:

$$s_w(x, t=0) = s_{wr}. \tag{6}$$

The inlet boundary is exposed to water, a continuous zero water pressure, and a capillary back pressure to oil P_{cbo} that can be positive or zero (Andersen et al. 2019a,d):

$$s_w(x=0^-, t) = 1, \qquad p_w(x=0, t) = 0, \tag{7}$$

(8) $$P_c(x=0^-,t)=\min\left(P_c\left(s_w(x=0^+,t)\right),P_{cbo}\right).$$

Scaled back pressure J_{bo} is related to P_{cbo} via (5). Increasing $P_{cbo}>0$ reduces any positive inlet oil pressure gradient towards zero reducing counter-current oil production. The oil flux *into* the core must be zero. The water entering aims to increase the saturation until the inlet capillary pressure is reached. If P_{cbo} is zero, this corresponds to a zero capillary pressure condition implicating a constant saturation boundary condition: $s_w(x=0^+,t)=s_{eq}$ (s_{eq} is the saturation where $P_c=0$). For a nonzero P_{cbo} the inlet saturation increases with time towards s_{eq}. The outlet is exposed to oil with zero oil pressure. Water pressure is discontinuous at this boundary and follows from the capillary pressure:

(9) $$s_w(x=L^+,t)=0,\qquad p_w(x=L^-,t)=-P_c\left(s_w(x=L^-,t)\right).$$

The system (1) to (9) of transport equations, boundary and initial conditions is strongly coupled: The transport equation (1) requires the total flux u_T to evaluate the advective term. u_T can be calculated by solving (2) for the water pressure distribution, which requires saturation distribution as input. Saturation directly affects the outlet boundary condition of water pressure (9), and changes with time. Due to this complexity, visualizing the solution and its change with input parameters is not straightforward. We will approximate this system to a simplified one allowing analytical evaluation and more direct interpretation.

Oil recovery factor is reported as the volume fraction of recoverable oil by SI at the outlet side (co-current recovery, RF^{co}), the inlet side (counter-current recovery, RF^{cou}) and overall (total recovery, RF):

(10) $$RF^{co}(t)=\frac{\frac{1}{L\phi}\int_{t'=0}^{t}u_T(x=L,t)dt}{s_{eq}-s_{wr}},$$

(11) $$RF(t)=\frac{\frac{1}{L}\int_{x=0}^{L}s_w(x,t)dx-s_{wr}}{s_{eq}-s_{wr}},$$

(12) $$RF^{cou}(t)=RF(t)-RF^{co}(t).$$

2.2. Analytical model for co-current spontaneous imbibition

The main assumption for generating the analytic solution is to ignore the capillary diffusion term in the transport equation. Capillary pressure still appears in the pressure equation and is the driving force.

(13) $$\phi\partial_t s_w=-u_T\partial_x f_w,$$

(14) $$\partial_x u_T=0,$$

(15) $$u_T=u_w+u_o=-K(\lambda_o\partial_x P_c+\lambda_T\partial_x p_w),$$

A saturation profile from BL theory (Buckley and Leverett 1942) is then obtained. As both the advective and diffusion terms originate from capillary forces during COC SI it is reasonable to expect they are of comparable magnitude. The capillary diffusion term is responsible for counter-current production and smoothing saturation gradients. This term's absence results in a sharper saturation profile, although comparable to the original solution (Andersen et al. 2019a). The advective term explains co-current production and predicts observed trends in imbibition rate and end recovery. Ignoring the diffusion term is motivated mainly by obtaining the explicit solution and that the advective term appears to hold more essential information. Although the BL solution typically describes forced displacement, we emphasize that the process is entirely capillary pressure driven. We set a fixed saturation s_{eq} at the inlet (corresponding to zero capillary pressure), and a zero water pressure:

(16) $$s_w(x=0,t)=s_{eq},$$

(17) $$p_w(x=0,t)=0.$$

and at the outlet:

(18) $$s_w(x=L^+,t)=s_{wr},$$

(19) $$p_w(x=L^-,t)=-P_c\left(s_w(x=L^-,t)\right).$$

Standard initial conditions of connate water saturation are applied:

(20) $$s_w(x,t=0)=s_{wr}.$$

The invariant shape of the BL solution assumes a semi-infinite system, while we consider a system where

water is stopped at the outlet. The last simulation cell would rapidly build up water saturation to its maximum value and give zero oil mobility. Oil production after front arrival is however observed experimentally and numerically since in the full solution capillary pressure gradient terms give a smoother rise in saturation. To handle this, the mass that would leave the system in a semi-infinite system is distributed within the closed system according to the BL profile.

Let t_c denote the time water reaches the outlet. 'Early time' is $t < t_c$ and 'late time' is $t > t_c$. The derivation of the early and the late time solution and special cases such as PLD are found in **Appendices A**, **B** and **C**, respectively. A brief summary of main features are given here. Recovery at early time relative to recovery at front arrival $RF(t_c)$ is expressed as:

$$RF/RF(t_c) = \frac{1}{\frac{\lambda_o(s_{wr})}{\lambda_T^*} - 1}\left[-1 + \sqrt{1 + \left[\left(\frac{\lambda_o(s_{wr})}{\lambda_T^*}\right)^2 - 1\right]\frac{t}{t_c}}\right] \tag{21}$$

$$t_c = \frac{\sqrt{\frac{\phi}{K}}L^2}{\sigma_{ow}} \frac{\frac{1}{2}\left[\frac{1}{\lambda_T^*} + \frac{1}{\lambda_o(s_{wr})}\right]}{f_w'(s_f)[J(s_{wr}) - \Delta J^*]}, \qquad RF(t_c) = \frac{s_f - s_{wr}}{s_{eq} - s_{wr}} \frac{f_w(s_{eq}) - f_w(s_{wr})}{f_w(s_f) - f_w(s_{wr})} \tag{22}$$

$$\Delta J^* = \int_{X=0}^{1} (1 - f_w)\partial_X J dX\,, \qquad \frac{1}{\lambda_T^*} = \int_{X=0}^{1} \frac{1}{\lambda_T} dX \tag{23}$$

λ_T^* is a characteristic total mobility, and $J(s_{wr}) - \Delta J^*$ is a characteristic scaled capillary pressure driving the SI process. Both are evaluated over the invariant BL saturation profile behind the front. These constants incorporate the saturation functions and fluid viscosities, while interfacial tension, porosity, permeability and length appear proportionally in the time scale. Two constant mobilities determine the flow resistance in the core; that of the oil downstream the front, $\lambda_o(s_{wr})$, and the effective mobility λ_T^* of the water-oil distribution upstream. The solution has same functional relation of recovery vs time as if PLD was assumed in the derivation, see (80) and (82). The differences are related to the specific values of the effective total mobility behind the front, the effective capillary pressure and the recovery when the front reaches the outlet. E.g., for PLD, λ_T^* is equivalent to total mobility evaluated at the imbibing saturation, $\lambda_T(s_{eq})$ and the driving capillary pressure will be $J(s_{wr})$ (if $f_w = f_w(s_{eq})$ and $J = J(s_{eq}) = 0$ then $\Delta J^* = 0$). With less favorable mobility ratio a distribution with $(1 - f_w)\partial_X J > 0$ follows, resulting in $\Delta J^* > 0$ and lower driving force. The profile saturations $s_f < s_w < s_{eq}$ define the interval where the saturation functions affect the solution. For favorable mobility ratio, the behavior is determined by a narrow saturation interval, while a greater saturation interval is important at less favorable mobility ratios. This principle was applied using numerical simulations to match experimental data in Andersen et al. (2019a). A PLD solution was derived by Haugen et al. (2014, 2015). Good match with experimental data was obtained although the underlying assumption of PLD should only be considered valid at favorable mobility ratios.

At early times the saturation profile behind the front is invariant and average saturation and recovery factor are then linearly related with front position. At late times the saturation profile changes relative to the foremost position (outlet) and the imbibition rate, average saturation and recovery are non-linearly related to the water saturation at the outlet s_{wR}. The driving force capillary pressure $J^{**}(s_{wR})$ and effective mobility $\lambda_T^{**}(s_{wR})$ are no longer constant, but functions of this saturation. The driving force is reduced to a capillary pressure in the saturation range above s_{wR}, decreasing with rising s_{wR}. The mobility of the system may increase if the mobility $\lambda_o(s_{wr})$ was low compared to λ_T^*.

2.3. Numerical solution

Simulations of the general system (1) to (9) were run using the core scale simulation software IORCoreSim (Lohne 2013), developed by the National IOR Centre of Norway. A 1D model was used, which was uniformly gridded into 200 cells in the axial direction. Saturation changes of $\Delta s_w = 0.002$ were used to limit the time steps in addition to frequent reporting. The model was implemented in line with the presented equations using Black Oil Model assumptions, with rock, oil and water as immiscible and

incompressible. The oil phase pressure distribution is evaluated at the new time step by linearizing the pressure equation with saturation dependent terms evaluated at the old time step. The saturation distribution at the new time step is found solving implicitly a transport equation for water (expressed in terms of fractional flow), where the saturation dependent functions are evaluated at the new saturations and the pressure dependent terms and total flux obtained from the pressure equation are held fixed. We refer to (Lohne 2013) for more details. The analytical solution described in Section 2.2 was implemented as a MATLAB code.

3. Results and discussion

3.1. Input data

Reference rock-fluid parameters are listed in **Table 1**, selected typical of water and decane at ambient conditions and outcrop chalk (Zeppieri et al. 2001; Andersen et al. 2018). The saturation functions were described using correlations from Andersen et al. (2017b) for scaled capillary pressure and Brooks and Corey (1966) for relative permeability:

$$J(s_w) = \frac{q_a}{1 + r_a S_w} - \frac{q_b}{1 + r_b(1 - S_w)} + q_c, \tag{24}$$

$$k_{rw}(s_w) = k^*_{rw}(S_w)^{n_w}, \qquad k_{ro}(s_w) = k^*_{ro}(1 - S_w)^{n_o}, \tag{25}$$

$$S_w = \frac{s_w - s_{wr}}{1 - s_{or} - s_{wr}}, \qquad (s_{wr} < s_w < 1 - s_{or}). \tag{26}$$

q_a, q_b, q_c, r_a, r_b are nonnegative dimensionless parameters for the J-function, while $k^*_{rw}, k^*_{ro}, n_w, n_o$ are nonnegative dimensionless Corey input parameters. s_{or}, s_{wr} represent the critical phase saturations and S_w is normalized water saturation. Two wetting states were considered, namely strongly water-wet (SWW) and mixed-wet (MW). At Darcy scale the saturation functions are commonly used to reflect wettability (Anderson 1987a,b; Behbahani and Blunt 2005; McPhee et al. 2015). SWW state is reflected in positive oil-water capillary pressure for all saturations, while MW refers to positive capillary pressure at low water saturations and negative capillary pressure at high water saturation. At positive capillary pressure values water displaces oil spontaneously, while for negative values forces such as gravity or advection must be applied to imbibe more water. Representative data in terms of scaled capillary pressure and relative permeabilities were taken from Bourbiaux and Kalaydjian (1990) for SWW and from Andersen et al. (2017a) for MW and the relevant parameters are listed in **Table 2**. The functions are plotted in **Figure 2** with focus on the saturation interval $s_{wr} < s_w < s_{eq}$ where spontaneous imbibition occurs.

Table 1 Reference input parameters.

Parameter	Values	Parameter	Values	Parameter	Values
L	10 cm	σ_{ow}	50 mN/m	J_{bo}	0
K	2 mD	μ_w	1 cP		
ϕ	0.4	μ_o	1 cP		

Table 2 Saturation function input parameters for the correlations (24) to (26).

Parameters	s_{wr}	s_{or}	k^*_{rw}	k^*_{ro}	n_w	n_o	q_a	q_b	q_c	r_a	r_b
SWW	0.40	0.43	0.045	0.43	1.8	1.4	1.77E-1	7.35E-2	7.30E-3	2	40
MW	0.05	0.20	0.3	1.0	4.5	2.0	9.87E-3	9.87E-3	8.35E-3	11.2	0

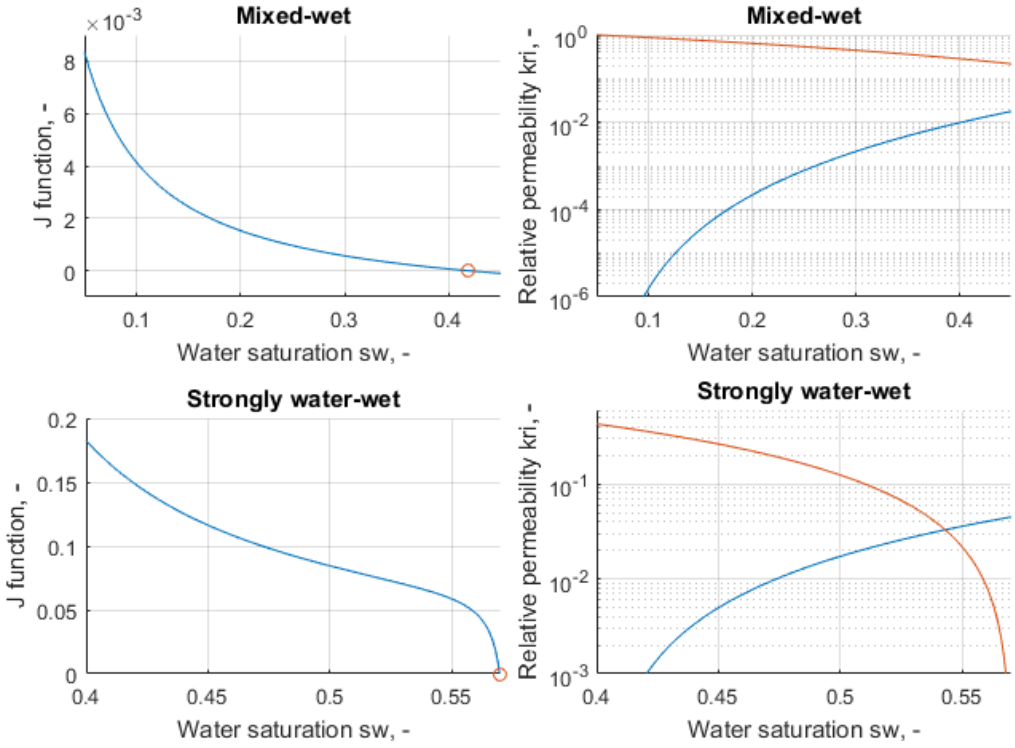

Figure 2 Input saturation functions in terms of scaled capillary pressure (left) and relative permeability (right) for MW (top) and SWW (bottom) cases. The front saturation s_f is marked on the capillary pressure functions which in both cases corresponds to the saturation s_{eq}.

3.2. Behavior of the analytical solution

Recovery factor RF is plotted based on the analytical solution in **Figure 3** for the SWW case with oil viscosity systematically varied by factors of ~3 from 0.1 to 1000 cP. The results are plotted against scaled time t/t_c in the top figure and absolute time in the bottom figure. The solution depends on the ratio of mobility $\lambda_o^{max}/\lambda_T^*$ between oil and the imbibing saturation profile. These values are indicated together with the mobility ratio $\lambda_o^{max}/\lambda_T^{eq}$ corresponding to PLD. The following is observed:

- At scaled time equal to 1 the front saturation reaches the outlet and the early time solution (full lines) switches to the late time solution (dashed lines). This transition is observed by a reduced imbibition rate, especially for low oil viscosities, while the transition is less apparent for high oil viscosities. In these cases the reduced driving force is compensated by improved mobility.
- The recovery at scaled time equal 1 systematically reduces with less favorable mobility ratio. This follows from the low saturations behind the front and was observed by Meng et al. (2017) and Andersen et al. (2019a).
- At early times the imbibition rate increases with time if $\frac{\lambda_o^{max}}{\lambda_T^*} < 1$ since the mobility of the system increases, while the driving force is constant. Similarly, if $\frac{\lambda_o^{max}}{\lambda_T^*} > 1$ the system mobility is reduced, and imbibition rate reduces. If $\frac{\lambda_o^{max}}{\lambda_T^*} \approx 1$ the imbibition rate is constant (linear recovery). This result follows mathematically from the analytical solution.
- For cases where oil mobility is negligible $\frac{\lambda_o^{max}}{\lambda_T^*} \ll 1$ the imbibition rate declines as a square root of time recovery profile, in accordance with e.g. Washburn (1921) and Li (2007), with mobility depending on water only.
- For $\frac{\lambda_o^{max}}{\lambda_T^*} \geq 1$ the two mobility ratios are very similar $\left(\frac{\lambda_o^{max}}{\lambda_T^*} \approx \frac{\lambda_o^{max}}{\lambda_T^{eq}}\right)$ which indicates PLD (the mobility of the moving saturation profile equals that of the profile with uniform max saturation

s_{eq}). The mobility ratio $\frac{\lambda_o^{max}}{\lambda_T^*}$ is associated with the evolution of imbibition and the case with $\frac{\lambda_o^{max}}{\lambda_T^*} = 1.1$ shows linear recovery as expected, but $RF\left(\frac{t}{t_c} = 1\right)$ is somewhat less than one (~0.93) while the cases with higher ratios show full recovery. This mobility ratio incorporates the entire saturation functions regardless of correlation form and could be a natural alternative to evaluate proximity to PLD together with mobility ratios evaluated only at the end points or at characteristic saturations. Nygård and Andersen (2020) presented a generalized mobility ratio accounting for all main simulation input parameters to evaluate water-alternating-gas performance. Berg and Ott (2012) evaluated stability of immiscible CO2 flooding and found that the mobility ratio evaluated at the BL front saturation was a better criterion than the end point mobility ratio.

Figure 4 shows the same example for the MW case, only that the oil viscosity range is from 1 to 10000 cP. The same observations hold, except that at low oil viscosities the recovery profiles converge at a curve below a square root of time profile, see **Appendix C.iii** for details.

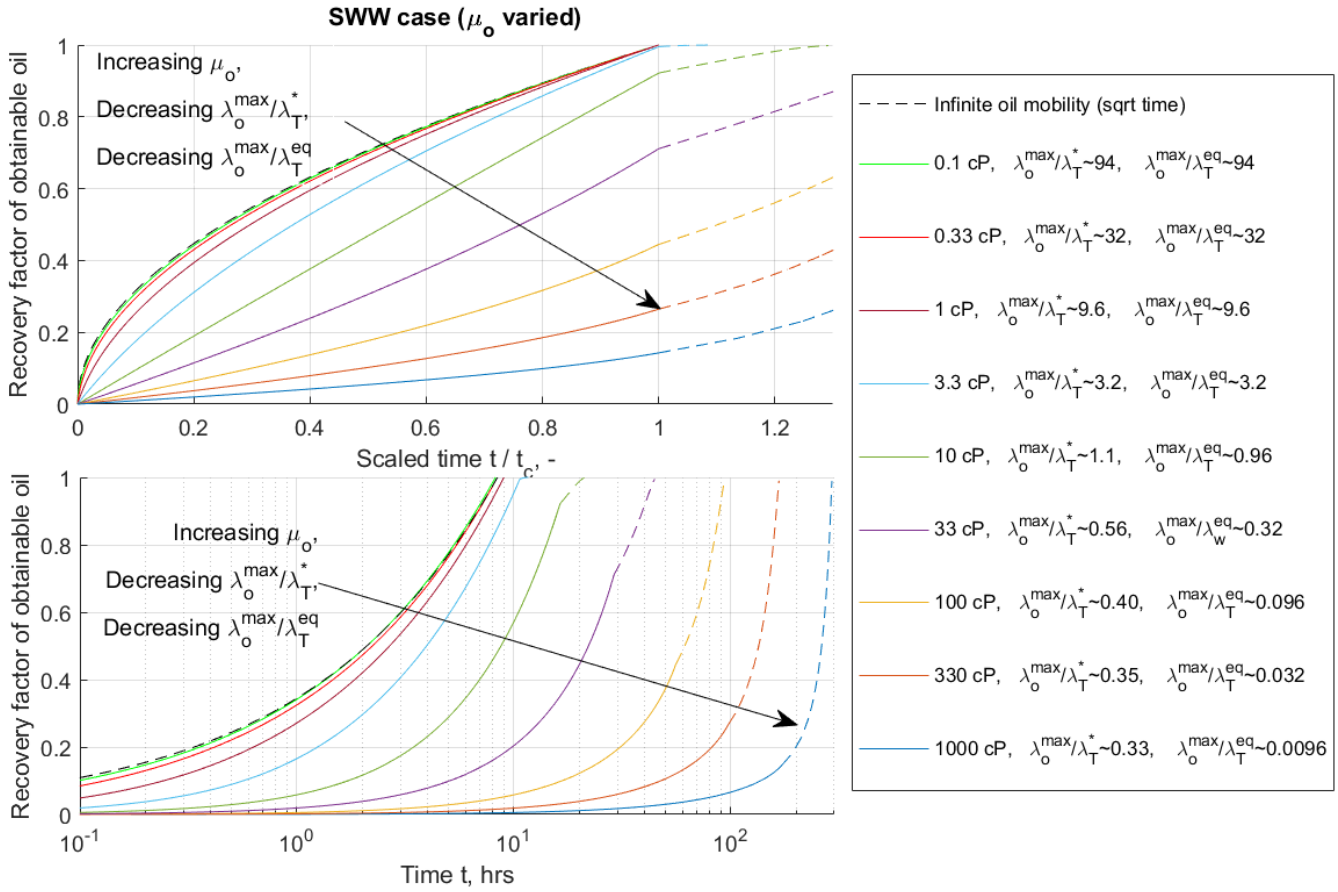

Figure 3 Analytical solution simulation results of oil recovery (RF) against scaled time (top) and absolute time (bottom) for the SWW case at early and late times. Oil viscosity was varied (by factors of ~3) from 0.1 cP (light green) to 1000 cP (dark blue). All other parameters were assigned reference values. Corresponding mobility ratios $\lambda_o^{max}/\lambda_T^*$ and $\lambda_o^{max}/\lambda_T^{eq}$ are indicated. At very low oil viscosity a square root of time recovery profile is obtained. The mobility ratio $\lambda_o^{max}/\lambda_T^*$ determines whether imbibition rate increases, decreases or is constant at early time.

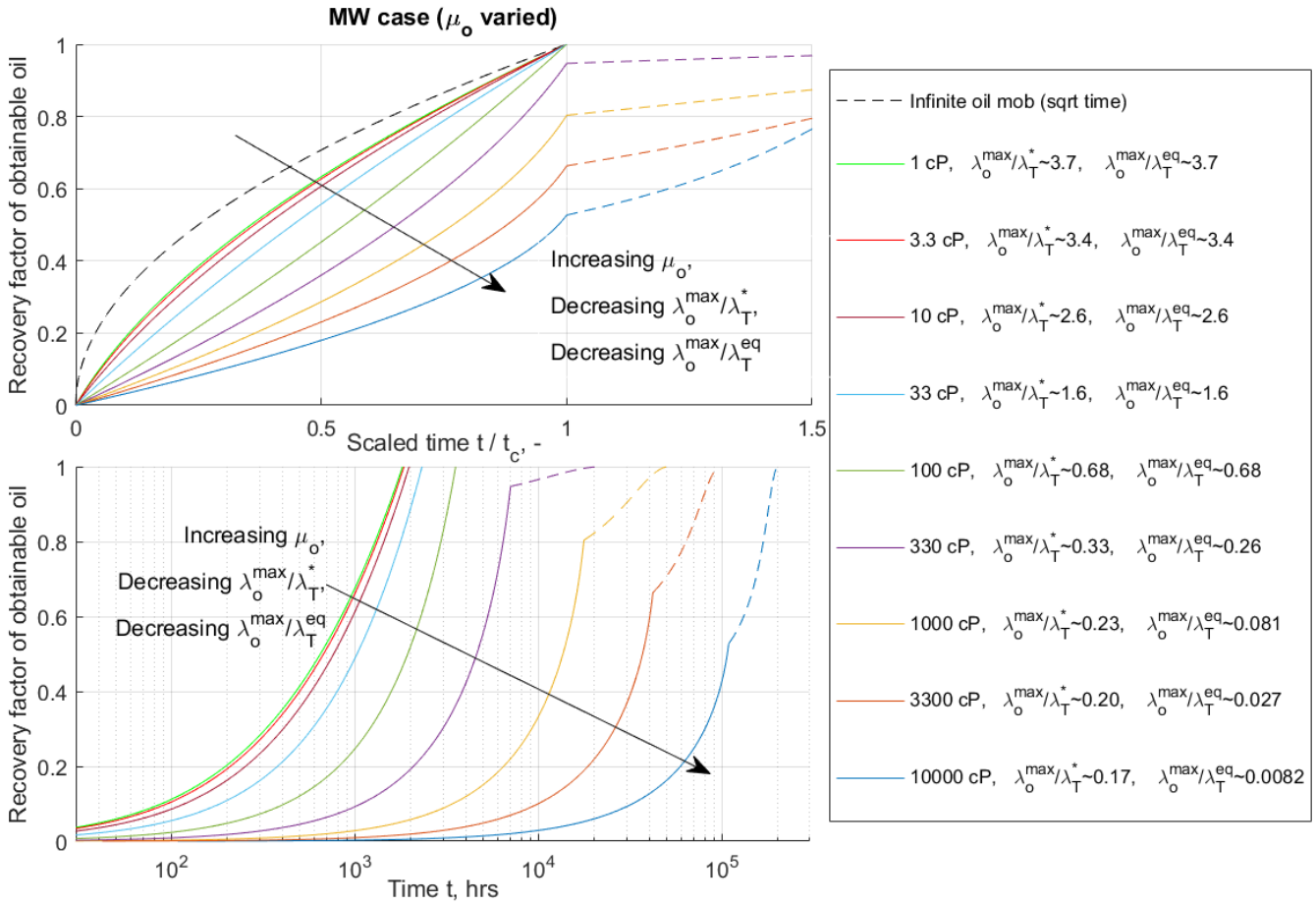

Figure 4 Analytical solution simulation results of oil recovery (RF) against scaled time (top) and absolute time (bottom) for the MW case at early and late times. Oil viscosity was varied (by factors of ~3) from 1 cP (light green) to 10000 cP (dark blue). All other parameters were assigned reference values. Corresponding mobility ratios $\lambda_o^{max}/\lambda_T^*$ and $\lambda_o^{max}/\lambda_T^{eq}$ are indicated. The mobility ratio $\lambda_o^{max}/\lambda_T^*$ determines whether imbibition rate increases, decreases or is constant at early time. The curves converge at low oil viscosity, but below a square root of time profile.

In **Figure 5** saturation profiles are shown for the SWW (100 cP) and MW (1000 cP) cases at $t = t_c$ (dark blue) and times with equally spaced outlet saturations. The SWW case has low recovery at t_c (ca 45%) due to the low saturation behind the front, while the MW case in this example has a higher recovery at t_c (ca 80%), also seen in **Figure 3** and **Figure 4** (yellow curves). The solution preserves the parts of the BL profiles with higher saturations than the outlet saturations.

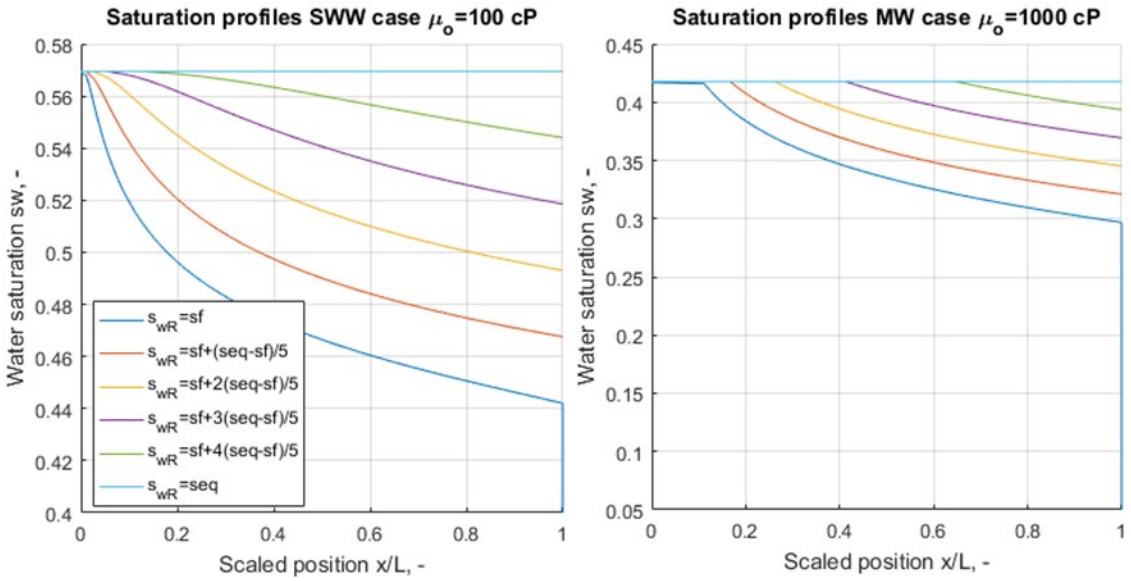

Figure 5 Saturation profiles for the SWW case with μ_o = 100 cP and the MW case for μ_o = 1000 cP at times corresponding to different levels of the water saturation at the outlet: from the outlet is reached to end recovery.

3.3. Comparison of analytical and numerical solutions

The analytical solution has implicitly assumed that the production is entirely co-current. Although the literature often suggests counter-current production is negligible, experimental and simulation works (Haugen et al. 2015; Meng et al. 2017; Andersen et al. 2019a) have also demonstrated significant counter-current production. By imposing a capillary back pressure, e.g. via a thin water-wet filter or porous disk, it is possible to eliminate counter-current production without hindering water from imbibing. We will compare the analytical solution to numerical solutions of (1) to (9) when (a) a zero or (b) a high scaled capillary back pressure J_{bo} is applied at the inlet. 'High' refers to a value above $J(s_{wr})$ to eliminate counter-current production.

3.3.1. Saturation profiles

In **Figure 6** saturation profiles are shown for MW and SWW cases at low and high oil viscosity, with high J_{bo} (dashed lines) and $J_{bo} = 0$ (full lines). The profiles are displayed at three identical times including times before and after the front has reached the outlet. The figures also contain BL saturation profiles (dashed/dotted lines) under same viscosity and saturation function conditions, displayed when the average saturation is identical to that of the numerical solution with $J_{bo} = 0$. The following is observed:

- The numerical solution profiles are both relatively smooth due to the capillary diffusion term, while the BL solution where the term was ignored is sharper with a clear front.
- The favorable mobility cases (1 cP viscosity) have the steepest saturation gradients and hence the strongest impact from the capillary diffusion term. The unfavorable mobility cases show closer resemblance between the numerical solution with $J_{bo} = 0$ and the BL profiles. A smooth front can be observed in all the numerical solutions which follows the trend of the BL solution, with front saturation decreasing with less favorable mobility ratio.
- Favorable mobility ratio is associated with negligible counter-current production. Eliminating it with J_{bo} hence results in no difference between the numerical solutions. At unfavorable mobility ratio (right hand side figures) the counter-current production is significant when $J_{bo} = 0$ and eliminating it delays the imbibition front.
- The numerical solutions with $J_{bo} = 0$ display a fixed saturation at the inlet s_{eq}, while the high J_{bo} solutions have a gradually increasing inlet saturation. For the latter case the inlet oil pressure varies according to eliminating the oil flux at the inlet. The water pressure remains zero, the inlet capillary pressure then varies and the saturation only slowly approaches s_{eq}.

- At late times both numerical solutions with high oil viscosity indicate accumulation of water saturation at the outlet and do not maintain the monotonous saturation gradient of the BL profile.

The resemblance between COC SI saturation profiles and BL profiles was also demonstrated in Andersen et al. (2019a). The smoothening effect of the capillary diffusion term was discussed by Andersen et al. (2017, 2019b) for cases where the imbibition rate into the core was limited by a porous disc or a low permeable gel. The capillary diffusion term then was more dominant resulting in more uniform saturation profiles.

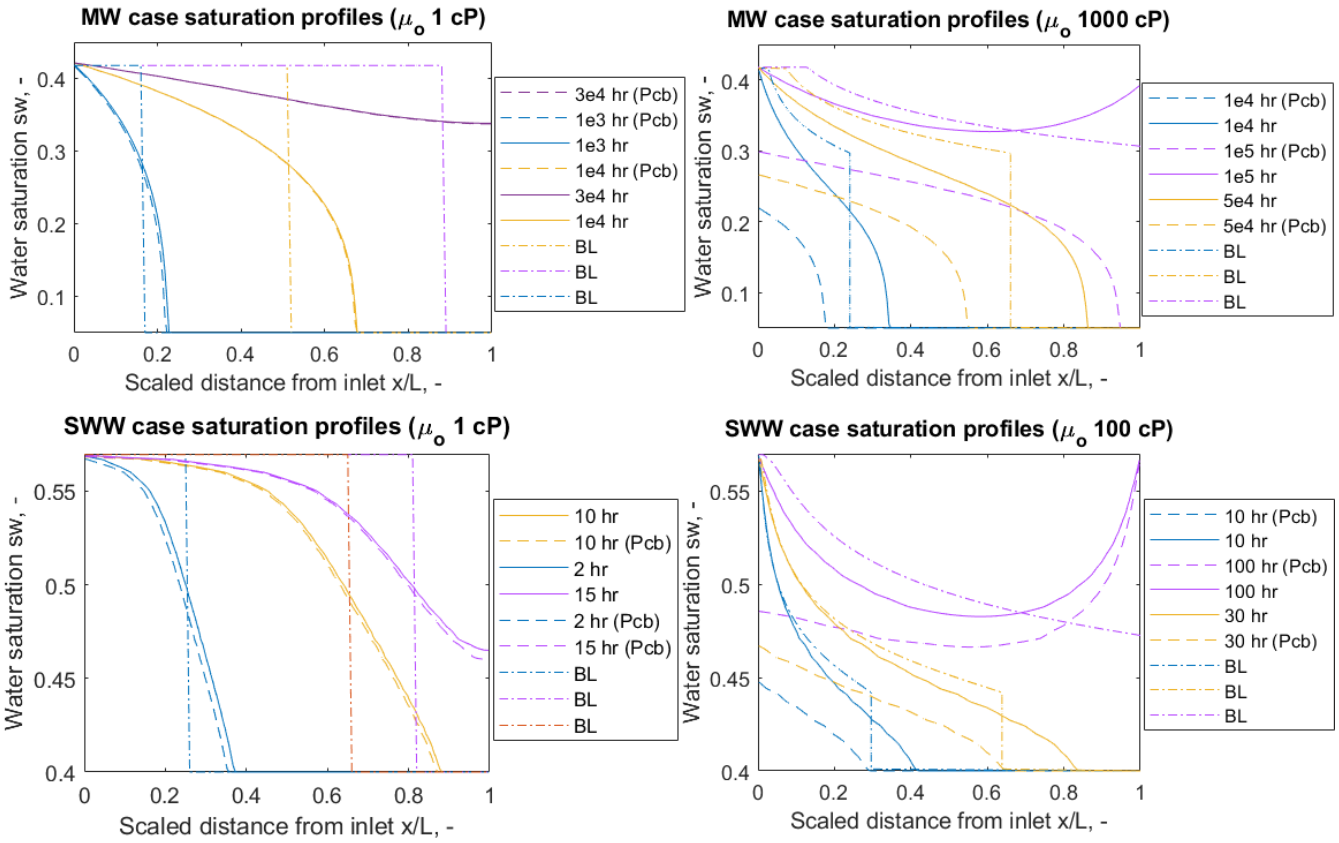

Figure 6 Saturation profiles from the numerical model for MW and SWW cases with $J_{bo} = 0$ (full lines), high J_{bo} (dashed lines) to stop counter-current production for high (100 or 1000 cP) and low (1 cP) oil viscosities at identical times. BL solutions are presented at identical average saturation as the $J_{bo} = 0$ solutions.

3.3.2. Recovery profiles and scaling

In **Figure 7** we see RF vs time for SWW cases with oil viscosities from 1 to 1000 cP. Numerical solutions with high J_{bo} (full lines) and $J_{bo} = 0$ (dashed lines) and analytical solutions (dotted/dashed lines, with the critical time marked by a circle) are displayed. We notice the following:

- For the numerical solutions, a high J_{bo} can significantly delay oil recovery compared to having $J_{bo} = 0$. For low oil viscosity of 1 cP the impact is negligible (since counter-current production is negligible), while it increases the time to reach the same recovery by a factor ~4 for 1000 cP oil viscosity (where counter-current production is significant for $J_{bo} = 0$). Regardless of J_{bo} and viscosity the imbibition rate of the numerical solutions is greatly reduced when the outlet is reached by the water front. The recovery profiles continue towards 1.
- At early times the analytical solutions and numerical solutions show comparable recovery profiles although the imbibition rate appears to be higher for the analytical solution. Most difference is seen at favorable mobility ratio (1 cP oil viscosity) where the analytical solution is ca twice as fast. The analytical solution overlaps better with the numerical solutions having high J_{bo} for cases with high oil viscosity (unfavorable mobility ratio). For the 1000 cP case, the profiles are identical until 200 h, near the critical time.

- The critical times of the analytical solution correspond well with when the numerical solutions show a sudden decrease in imbibition rate (referred to as 'breakthrough'). A factor of ~2 or less separates the times. Recovery at the critical time of the analytical solution and at imbibition rate decline in both numerical solutions differs by 0.05 to 0.15. For all solutions recovery at this event declines with increased oil viscosity (less favorable mobility ratio) in accordance with the BL profile.

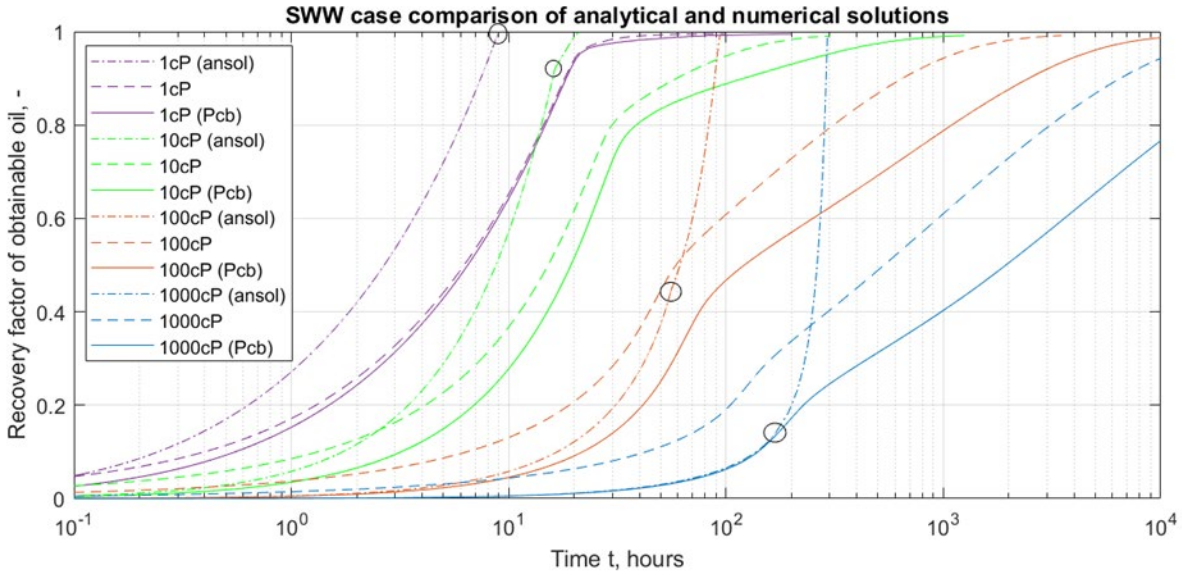

Figure 7 Recovery factor (RF) for SWW cases where oil viscosity was varied from 1 to 1000 cP using the analytical solution (dashed/dotted lines, 'ansol') and numerical simulations with a zero (dashed lines) or high capillary back pressure (full lines, 'Pcb') to allow or eliminate inlet counter-current production. The critical time and corresponding recovery calculated for the analytical solution are indicated by circles.

The numerical cases in the above example span time almost three orders of magnitude for a given recovery. Co-current and counter-current recovery (RF^{co} and RF^{cou}) for the numerical solution with $J_{bo} = 0$ are plotted against scaled time t/t_c (t_c calculated from the analytical solution) in **Figure 8**. This collects the 'breakthrough' events (a fall in co-current imbibition rate) to scaled times between 0.8 (for 1000 cP) and 2.2 (for 1 cP). It occurs exactly at scaled time 1 for the analytical solution. The difference between the analytical and numerical solution can be attributed to counter-current production and capillary diffusion within the system. The term $-K\lambda_o\partial_x P_c$ in the equation for imbibition rate u_T, see (3), is negative (the capillary pressure gradient is positive) and lowers the imbibition rate. Hence, a lower capillary pressure gradient reduces u_T. For cases with favorable mobility ratio the steep BL profile compared to the smooth numerical profile results in a faster imbibition rate for the analytical solution. For unfavorable mobility ratio the saturation profiles in the core are more comparable (see **Figure 6**) causing less impact on the calculation of u_T, but the initial fast counter-current production (which may exceed co-current production in the very beginning), see **Figure 8**, explains why the analytical solution for those cases first is slower than the numerical. As counter-current recovery stabilizes, the sharpness of the BL profile eventually dominates resulting in higher imbibition rate of the analytical than numerical solution.

Although the recovery curves are collected well according to breakthrough we note that the distinct shapes and separation into co- and counter-current production do not allow collecting the curves to one identical scaled curve as is possible for COUC SI (Ma et al. 1997; Schmid et al. 2011; Andersen et al. 2020a). However, the mobility ratio $\lambda_o^{max}/\lambda_T^*$ is seen in **Figure 8** to characterize co-current recovery for the numerical solution just as predicted by the analytical solution: when $\frac{\lambda_o^{max}}{\lambda_T^*} \approx 1$ the rate is constant, when $\frac{\lambda_o^{max}}{\lambda_T^*} > 1$ the rate decreases and when $\frac{\lambda_o^{max}}{\lambda_T^*} < 1$ the rate increases with time.

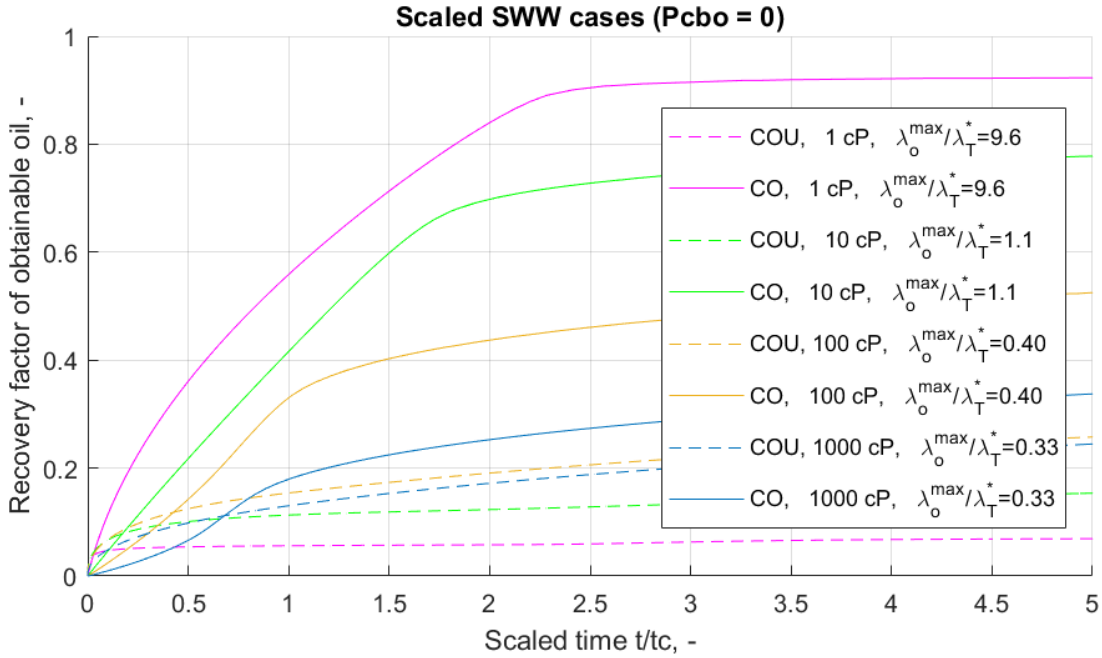

Figure 8 Co-current and counter-current recovery factors (RF^{co} and RF^{cou}) against scaled time for the SWW case with oil viscosities 1 to 1000 cP based on the numerical solution with $J_{bo} = 0$. Co-current recovery rate increases, decreases or is constant according to the mobility ratio $\lambda_o^{max}/\lambda_T^*$. The scaled solutions display breakthrough times between ~0.8 and 2.2. NB: Due to scaling the counter-current production at 100 cP appears higher than at 1000 cP, but it catches up and is systematically higher in absolute time.

The above example is repeated for MW cases where oil viscosity is varied with values 1, 100, 1000 and 10000 cP. RF vs time for analytical solutions and numerical solutions with zero and high J_{bo} is shown in **Figure 9.** Again, the two numerical solutions converge at favorable mobility ratio (low oil viscosity), while a high back pressure results in delay at unfavorable mobility ratio. The recovery at breakthrough decreases for less favorable cases. Compared to the previous example, there appears to be greater difference between the analytical and numerical solutions for low oil viscosities. As before the difference reduces at higher viscosity indicating the influence of the diffusion term diminishing with smoother saturation profiles.

RF^{co} and RF^{cou} vs scaled time for the numerical solution with $J_{bo} = 0$ are shown in **Figure 10**. Scaling the solutions should shift the breakthrough events of co-current recovery to a scaled time of 1. That appears reasonable at unfavorable mobility ratio (2.5 for 10000 cP and 5 for 1000 cP), although the favorable mobility cases deviate more from this (scaled time 10 for 100 cP and 20 for 1 cP). The conclusions regarding the dependence of co-current imbibition rate u_T on mobility ratio $\frac{\lambda_o^{max}}{\lambda_T^*}$ appear to hold.

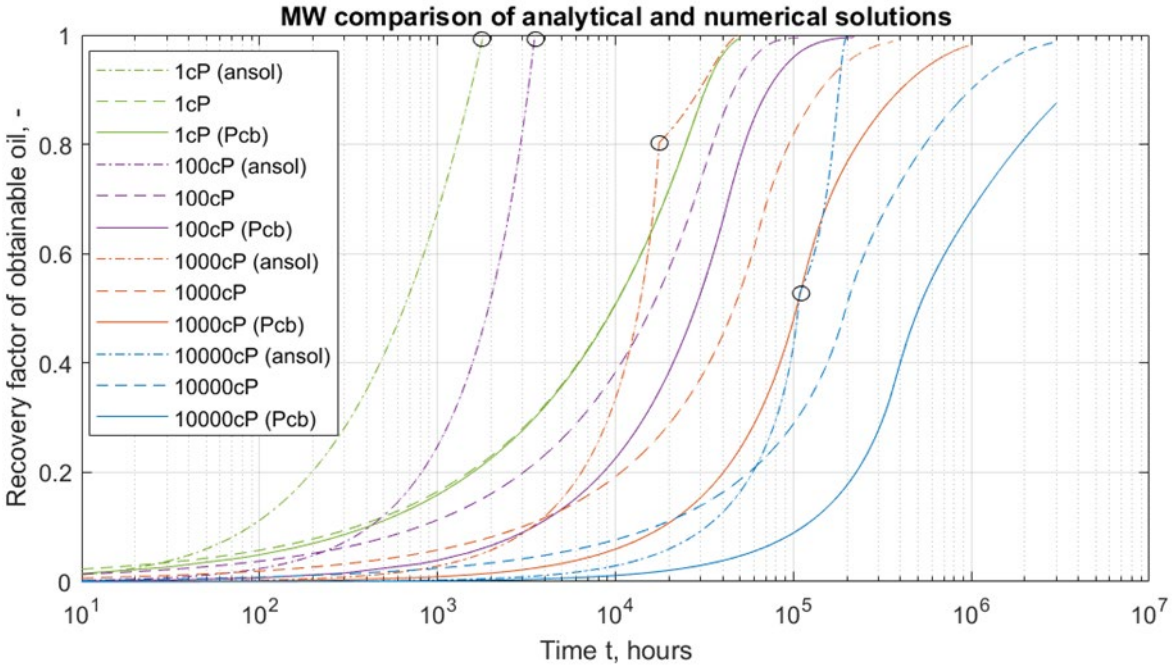

Figure 9 Recovery factor (RF) for MW cases where oil viscosity was varied from 1 to 10000 cP (except 10 cP) using the analytical solution (dashed/dotted lines, indicated by 'ansol') and numerical simulations either with $J_{bo} = 0$ (dashed lines) or high J_{bo} (full lines, indicated by 'Pcb'). The calculated critical time and corresponding recovery for the analytical solution is indicated by circles.

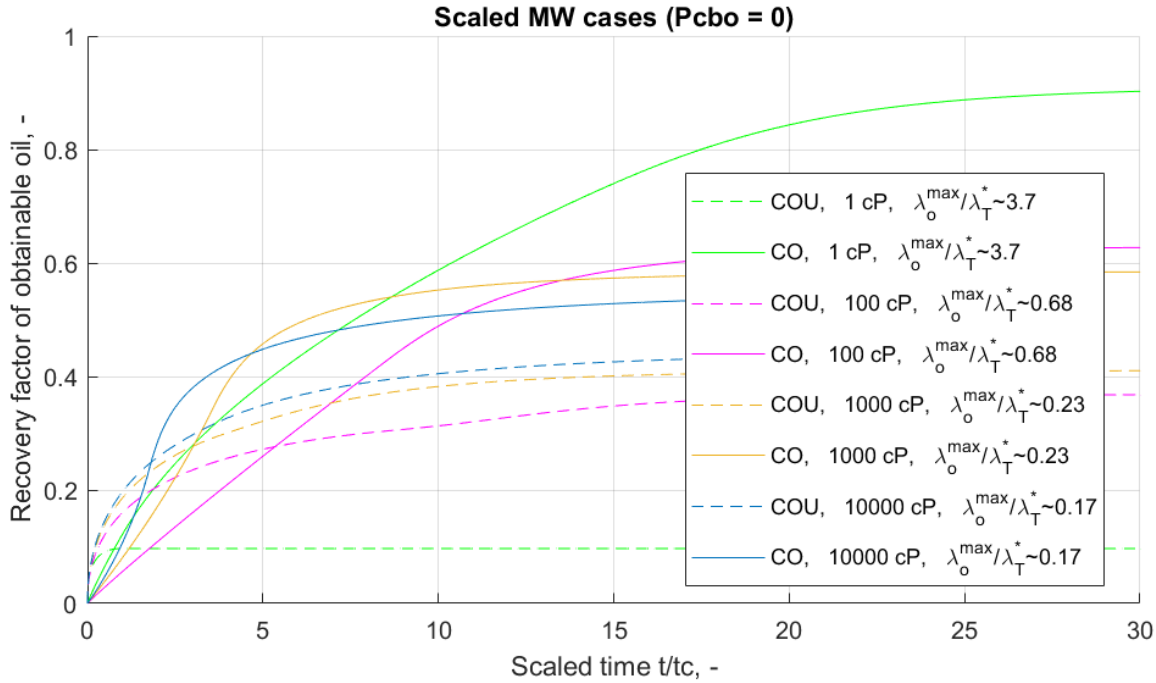

Figure 10 **Co-current and counter-current recovery factors $(RF^{co}$ and $RF^{cou})$ against scaled time for the MW case with oil viscosities 1 to 10000 cP (except 10 cP) based on the numerical solution with $J_{bo} = 0$. Co-current recovery rate increases, decreases or is constant according to the mobility ratio $\lambda_o^{max}/\lambda_T^*$.**

3.3.3. Scaling length

It is a direct outcome of the analytical solution that regardless of whether the solution is PLD or a continuous BL saturation profile, considers MW or SWW systems, early or late times, the time scale is directly proportional to $\frac{L^2\sqrt{\frac{\phi}{K}}}{\sigma_{ow}}$, see (50), (68), (70), (79) or (83). In other words, given the same saturation functions and viscosities the same shape of the solution will be obtained in terms of spatial or time profiles.

A system with variation in length, porosity, permeability or interfacial tension will need more or less time proportionally with the stated factor to obtain same results.

To see whether this holds in general, and not only for the analytical solution, numerical solutions (with $J_{bo} = 0$) were generated for three cases where MW and SWW states and low (1 cP) and high (100 cP) oil viscosity were applied and the system length was varied using values 10, 20, 40 and 80 cm. RF plotted against time is shown in the left side of **Figure 11**. The length variation gives a time span in the results of ca two orders of magnitude. In the right side of the figure the same results are plotted where the time is divided by length squared. This causes the profiles to collapse to a single curve and demonstrates that the COC SI process scales by the square length of the system.

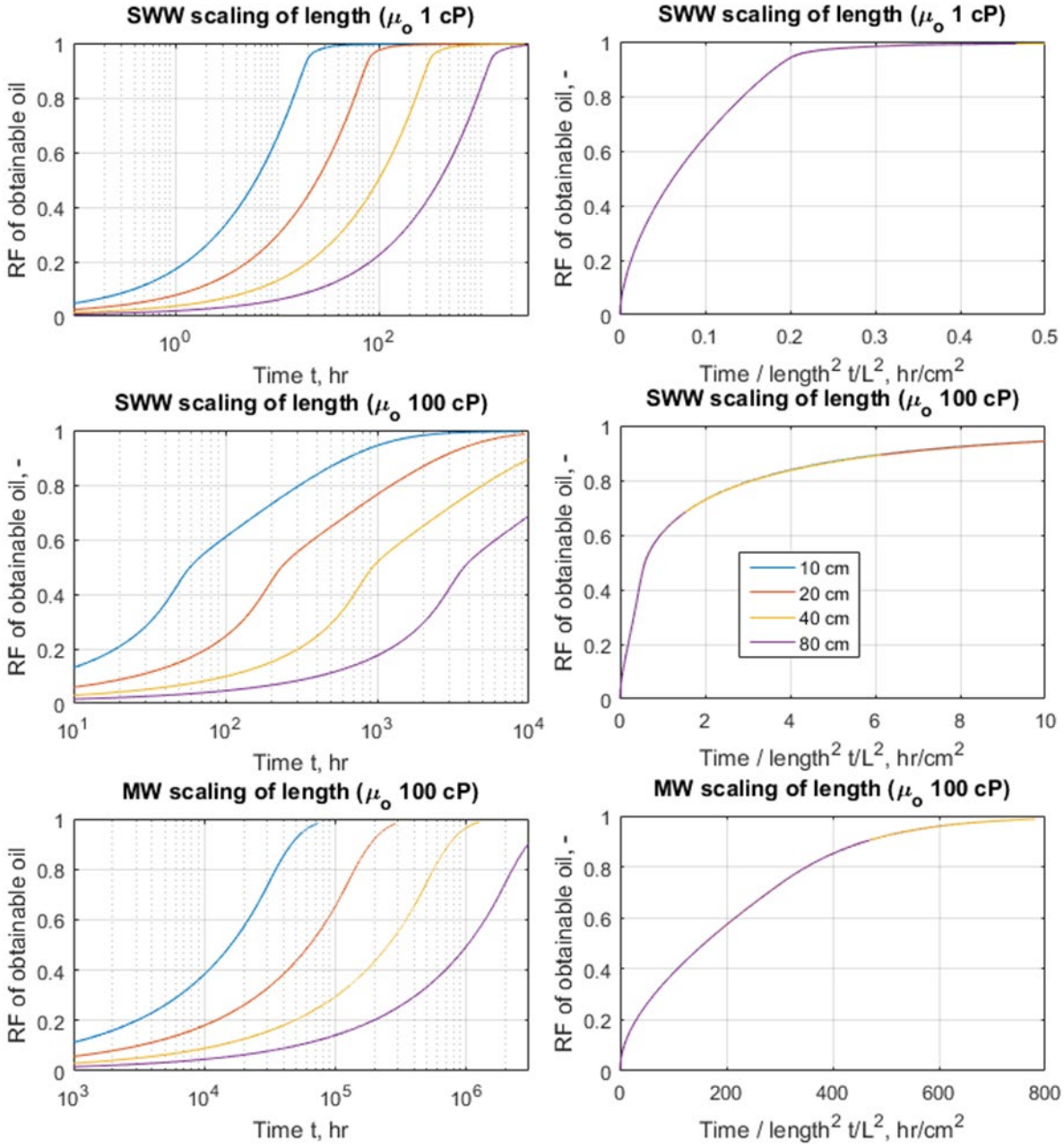

Figure 11 Numerical simulations (with $J_{bo} = 0$) used for scaling length with SWW or MW cases and viscosity of 1 or 100 cP (indicated above the figure). Four lengths were applied from 10 to 80 cm. Recovery factor (RF) is plotted against time (left) and time divided by length squared (right). Recovery scales with length squared for early and late time and for different wetting and mobility states.

3.3.4. Scaling saturation functions

Finally, we mention that the analytical solution suggests how different combinations of saturation

functions and viscosities can be scaled. Combinations giving same mobility ratio $\lambda_o^{max}/\lambda_T^*$ are predicted to give same recovery profile with scaled time towards the recovery obtained at t_c. This is demonstrated by considering the resemblance between **Figure 3** and **Figure 4** although we remark that the specific recovery at t_c will depend on the BL saturation profile. As we have seen, although the scaling is perfect for the analytical solution, the event when water reaches the outlet in the numerical solutions (and expectedly experimental data) is more diffuse and less accurate due to the mechanisms missing in the analytical solution. The breakthrough time in the previous examples was higher than the predicted (critical time) by a factor of 1 to 20. Better comparison of experimental data or numerical simulations may require that the applied critical time is that of the observed breakthrough event rather than the predicted one.

To evaluate whether data of different wetting states can be compared we plot co-current recovery of numerical solutions (with $J_{bo} = 0$) and recovery of analytical solutions until water reaches the outlet. This event was evaluated by a sudden decline in co-current rate for the numerical solution and calculated exactly for the analytical solution. Time was normalized against this breakthrough time and recovery was normalized against the recovery at that time. MW and SWW datasets are used with oil viscosities selected to give mobility ratios of three values: $\frac{\lambda_o^{max}}{\lambda_T^*} = \sim 3.5, 1, 0.33$. The results are shown in **Figure 12**. They demonstrate a clear correspondence with mobility ratio where a ratio of 1 indicates linear recovery, a high (favorable) value indicates declining imbibition rate and a low value (unfavorable) indicates rising imbibition rate. The analytical solutions overlap very well and agree with the numerical solutions of the SWW case. The numerical solution of the MW case shows higher recovery than the other solutions for the high and low mobility ratio, but overall the data group well according to the mobility ratio.

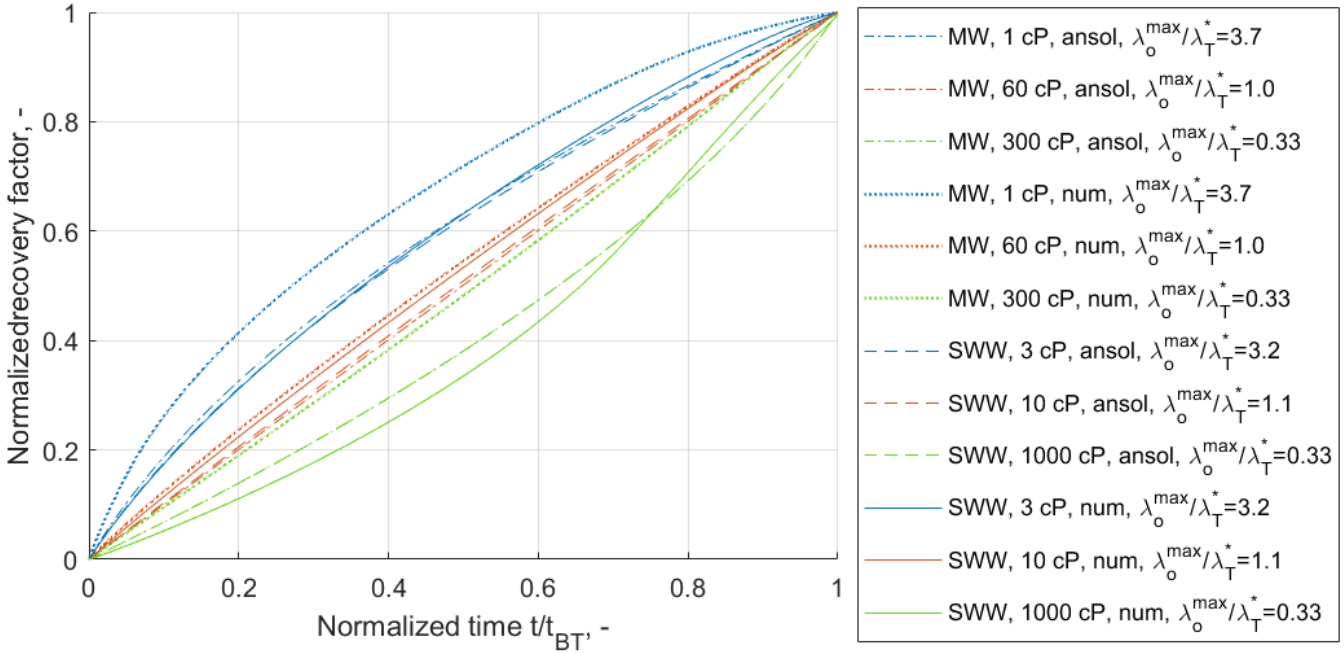

Figure 12 Co-current recovery for numerical solutions (with $J_{bo} = 0$) and recovery for analytical solutions normalized by their recovery at breakthrough (when water reaches the outlet) plotted against time normalized by the breakthrough time of the respective solutions. Both MW and SWW sets are applied with viscosities selected to give similar mobility ratios: ~3.5, 1, 0.33.

3.4. Interpretation of experimental data

The analytical model was used to match experimental data from Haugen et al. (2014) where system length was varied from 6 to 16.6 cm and other properties were $\mu_w = 1.09$ cP, $\mu_o = 1.47$ cP, $\phi \approx 0.47$, $K \approx 5$ mD and we assume $\sigma_{ow} = 0.035$ N/m. Total recovery vs time was matched, see **Figure 13,** by tuning the saturation function correlations (24) to (26). The model predicts that the model is invariant to length except in time scale. Hence, by matching only experiment CHP3 (10.5 cm), the four other experiments were predicted close to perfectly in shape and time scale. To match the tests it was noted that the imbibition

rate was declining with time indicating favorable mobility ratio. Brine then displaces oil piston-like and residual saturation corresponds to the last point. The mobility ratio was constant (invariant with length), and only depended on the k_{ri} end points. $k_{ro}^{max} = 1$ due to full initial oil saturation and hence only k_{rw}^{max} was needed to fit the evolution of the imbibition rate. As the slope was flatter than a square root profile, k_{rw}^{max} was determined accurately and the time scale followed from the end point of the J-function. We note that the saturation functions at intermediate saturations are uncertain from only these data and other functions giving same end points and PLD would give similar match.

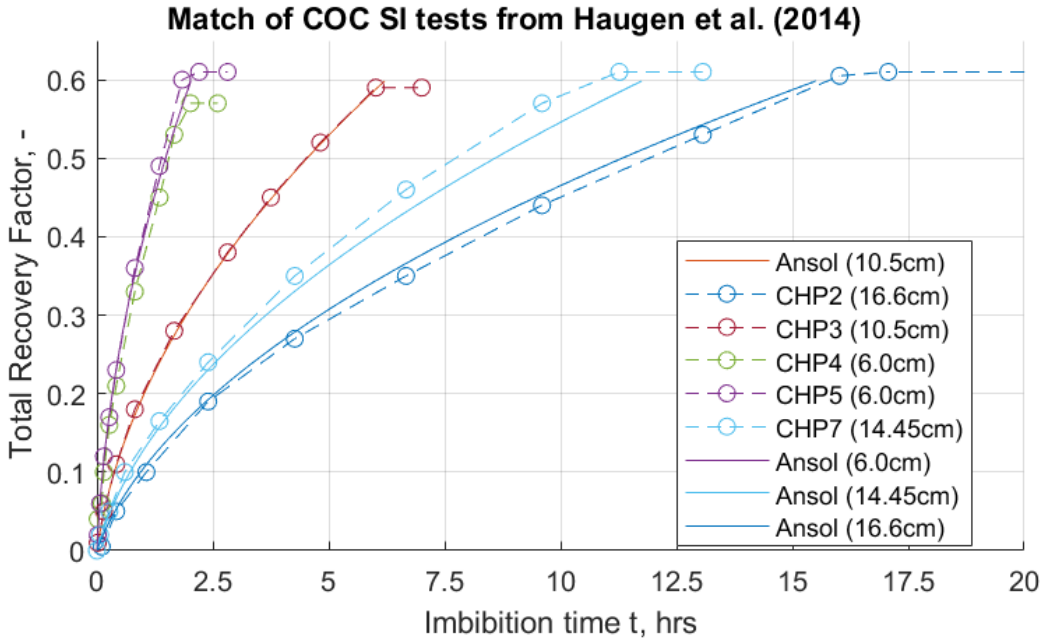

Figure 13 Comparison of experimental total recovery from Haugen et al. (2014) and matched analytical solution.

We also match data from Meng et al. (2017) where non-wetting phase viscosity was varied from 0.018 to 103.4 cP and other properties were $L = 0.41$ m, $\mu_w = 1$ cP, $\phi = 0.34$, $K \approx 2450$ mD, $\sigma_{gw} = 0.072 \frac{\text{N}}{\text{m}}$, $\sigma_{ow} \approx 0.035 \frac{\text{N}}{\text{m}}$. Using the same saturation functions the time scale for water to reach the outlet, the recovery at that time and the shape of the profiles in general are well matched. Increased non-wetting viscosity increases the time scale, causes the imbibition rate to go from decreasing with time to increasing with time, and lowers the recovery when water reaches the outlet. To match the data, the highly favorable mobility test (air) provided the residual non-wetting saturation. k_{ro}^{max} was again 1. The air mobility was practically infinite, so the water relative permeability end point and J-function end point in combination determined the time scale of that test. The relative permeabilities were selected to give right level of recovery for the different viscosities; a high fractional flow function follows high viscosity and gives low recovery at water arrival at the outlet based on the BL profile. Low mobilities increased the time, but could be compensated by raising the J-function. Some tuning of all three functions resulted in the final match. The saturation functions matching this and the previous dataset are shown in **Figure 15**.

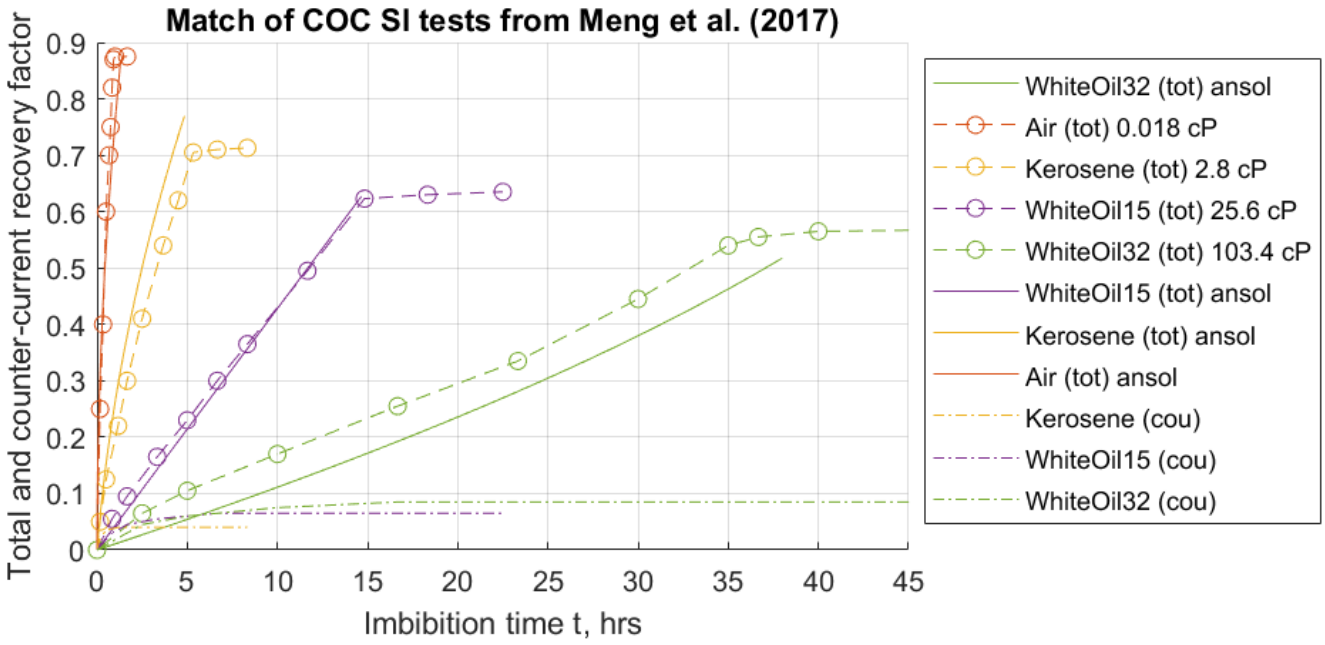

Figure 14 Total and counter-current recovery factor from experiments in quartz sand packs by Meng et al. (2017) compared to matched total recovery by the analytical solution.

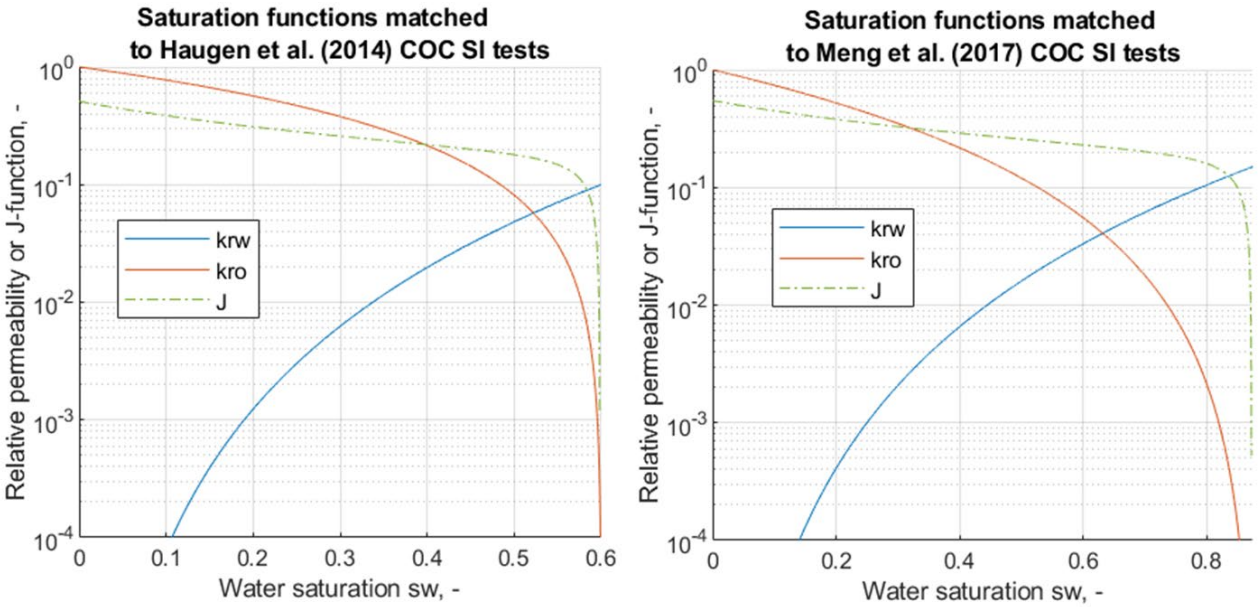

Figure 15 Saturation functions obtained matching the experiments by Haugen et al. (2014) and Meng et al. (2017) with the analytical solution.

4. Conclusions

An analytical model was derived for 1D co-current spontaneous imbibition (COC SI). The main assumption was that the capillary diffusion term could be neglected in the transport equation such that Buckley-Leverett (BL) profiles were obtained and counter-current production was ignored. Capillary pressure in the pressure equation was driving the process. The model accounts for wetting, saturation functions and viscosities, early time (before water reaches the outlet) and late time (after). Under the assumptions of the model, we conclude:

1) The (critical) time for water to reach the outlet was obtained explicitly and used to scale the solutions.

2) COC SI scales according to $\frac{L^2\sqrt{\frac{\phi}{K}}}{\sigma_{ow}}$ both at early and late time.

3) The saturation functions are incorporated in a characteristic total mobility and capillary pressure. They are both constant at early time, while they change dynamically at late time.
4) COC SI does not generally display a recovery profile proportional to square root of time as suggested by previous analytical solutions, except as an approximation when the non-wetting phase mobility is very high compared to that of the wetting phase. The square root of time profile is the most extreme curvature of the recovery profile.
5) A new mobility ratio was derived between initial oil mobility and the characteristic total mobility of the imbibing saturation profile; $\lambda_o^{max}/\lambda_T^*$. Analytically; at a ratio of 1, recovery is linear with time, at favorable mobility ratio (>1) imbibition rate decreases with time, while at unfavorable mobility ratio (<1) imbibition rate increases with time. For mobility ratio at 1 or higher, most or all obtainable oil was recovered at front arrival, indicating piston-like displacement. For values below 1, less than all the recoverable oil is produced at critical time.
6) Experimental data could be matched with the analytical solution.

The following was concluded when comparing results of the analytical model to those of full numerical simulations:

1) The numerical simulations verified that COC SI scales with length squared both at early and late times.
2) The critical time from the analytical solution successfully estimated, for the majority of the numerical solutions, the event of rapidly declining imbibition rate (water reaching the outlet). The time scale lets us estimate when the most available oil has been produced. Although production continues, the rate is much lower.
3) There was excellent correspondence in rise, decline or constant value of co-current imbibition rate with the new mobility ratio $\lambda_o^{max}/\lambda_T^*$ being <1, >1 or ≈ 1, respectively.
4) The analytical solution showed too high imbibition rate compared to the numerical solution for favorable mobility ratios. The capillary diffusion term is important at favorable mobility ratio due to the strong saturation gradients and the resulting smoothened profile yields a lower imbibition rate from the pressure equation.
5) The analytical solution showed too low imbibition rate compared to the numerical solution at early times for unfavorable mobility ratios. That is due to not accounting for rapid early counter-current production.
6) The analytical solution predicted too high imbibition rate at late times compared to the numerical solution because the BL profile does not capture the oil mobility restriction at the outlet at late times.

Acknowledgments

The author acknowledges the Research Council of Norway and the industry partners, ConocoPhillips Skandinavia AS, Aker BP ASA, Vår Energi AS, Equinor ASA, Neptune Energy Norge AS, Lundin Norway AS, Halliburton AS, Schlumberger Norge AS, and Wintershall DEA, of The National IOR Centre of Norway for support.

Appendix: Analytical solution

A. Early time solution

'Early time' is before water has reached the outlet. Applying the method of characteristics to (13) and noting that u_T is not constant in time, $s_w(x,t)$ is given by:

$$x(s_w) = \frac{1}{\phi} f'(s_w) \int_{\tau=0}^{t} u_T(\tau) d\tau, \qquad (s_f < s_w < s_{eq}), \tag{27}$$

$$x_f = \frac{1}{\phi} f'(s_f) \int_{\tau=0}^{t} u_T(\tau) d\tau, \qquad (s_{wr} < s_w < s_f), \tag{28}$$

$$s_w = s_{wc}, \qquad (x > x_f), \tag{29}$$

where s_f is the unique front saturation, determined by solving:

(30) $$f_w'(s_f) = \frac{f_w(s_f) - f_w(s_{wr})}{s_f - s_{wr}}, \qquad (s_f \in [s_{wr}, s_{eq}])$$

The $'$ refers to saturation differentiation. It is assumed in this and the following section a solution s_f from (30) exists. If no solution for s_f exists in this interval, we have PLD ($s_f = s_{eq}$ and s_w is uniformly equal s_{eq} behind the front), see Section C.ii. The saturation profile (27) to (29) is explicitly determined for any viscosities and relative permeabilities giving the flow function f_w. Only s_f may need to be determined numerically from (30). The profile at a specific time, given f_w, only depends on the total imbibed volume, not how imbibition rate changes with time. The profile can be distinguished into two regions:

- $0 < x < x_f$: where the continuous BL solution applies and there is a nonzero saturation gradient.
- $x_f < x < L$: where only mobile oil exists and there is zero saturation gradient.

$x_f = x(s_f)$ is the water front position, dividing the two regions by a saturation front. We scale position relative to the front:

(31) $$X = \frac{x}{x_f(t)} = \frac{f_w'(s_w)}{f_w'(s_f)}, \qquad dX = \frac{dx}{x_f(t)}$$

In the two regions total velocity is then given by:

(32)
(33) $$u_T = -K\lambda_T(s_w)\frac{1}{x_f}\partial_X p_w - K\lambda_o(s_w)\frac{1}{x_f}\partial_X P_c(s_w), \qquad (0 < \mathrm{X} < 1)$$

(34) $$u_T = -K\lambda_o(s_{wr})\frac{1}{x_f}\partial_X p_w, \qquad \left(1 < X < \frac{L}{x_f}\right)$$

Inlet water pressure p_{wL} is zero and since the water has not reached the outlet, the outlet water pressure p_{wR} is fixed corresponding to the zero oil pressure and initial saturation:

(35) $$p_{wL} = 0,$$

(36) $$p_{wR} = -P_c(s_{wr}), \qquad (x_f < L)$$

The pressure gradients in each region are:

(37) $$\partial_X p_w = -\frac{\lambda_o}{\lambda_T}\partial_X P_c - x_f\frac{u_T}{K\lambda_T}, \qquad (0 < \mathrm{X} < 1)$$

(38) $$\partial_X p_w = -x_f\frac{u_T}{K\lambda_o(s_{wr})}, \qquad \left(1 < X < \frac{L}{x_f}\right)$$

Note that the pressure gradient is constant in the oil region. The pressure drops in the two intervals are calculated:

(39) $$p_{wf} - p_{wL} = -\sigma_{ow}\sqrt{\frac{\phi}{K}}\int_{X=0}^{1}(1 - f_w)\partial_X J dX - \frac{x_f u_T}{K}\int_{X=0}^{1}\frac{1}{\lambda_T}dX,$$

(40) $$p_{wR} - p_{wf} = -\frac{u_T}{K\lambda_o(s_{wr})}(L - x_f),$$

p_{wf} is the water pressure at x_f. For known viscosities and saturation functions k_{rw}, k_{ro}, P_c (which leads to defined functions f_w and λ_T) the function integrals are constants and we introduce the notations:

(41) $$\Delta J^* = \int_{X=0}^{1}(1 - f_w)\partial_X J dX, \qquad \frac{1}{\lambda_T^*} = \int_{X=0}^{1}\frac{1}{\lambda_T}dX$$

where we note that $\lambda_T^* > 0$ and $\Delta J^* > 0$ are constant regardless of front position and time. (39) can then be written as:

(42) $$p_{wf} - p_{wL} = -\sigma_{ow}\sqrt{\phi/K}\,\Delta J^* - \frac{x_f u_T}{K\lambda_T^*},$$

We make use of the boundary conditions (35) and (36) in (40) and (42) giving:

(43) $$p_{wf} = -\sigma_{ow}\sqrt{\frac{\phi}{K}}\Delta J^* - x_f\frac{u_T}{K\lambda_T^*},$$

$$-\sigma_{ow}\sqrt{\phi/K}\,J(s_{wr}) - p_{wf} = -\frac{u_T}{K\lambda_o(s_{wr})}\left(L - x_f\right), \tag{44}$$

Eliminating p_{wf} we obtain imbibition rate as function of front position:

$$u_T = \sigma_{ow}\sqrt{\phi K}\,\frac{[J(s_{wr}) - \Delta J^*]}{\frac{x_f}{\lambda_T^*} + \frac{\left(L - x_f\right)}{\lambda_o(s_{wr})}}. \tag{45}$$

From (28) we relate x_f and u_T:

$$\frac{dx_f}{dt} = \frac{1}{\phi} f'\left(s_f\right) u_T, \tag{46}$$

which inserted into (45) gives:

$$\frac{dx_f}{dt}\frac{\phi}{f_w'\left(s_f\right)} = \sigma_{ow}\sqrt{\phi K}\,\frac{[J(s_{wr}) - \Delta J^*]}{\frac{x_f}{\lambda_T^*} + \frac{\left(L - x_f\right)}{\lambda_o(s_{wr})}} \tag{47}$$

We separate variables:

$$\left[\frac{x_f}{\lambda_T^*} + \frac{\left(L - x_f\right)}{\lambda_o(s_{wr})}\right] dx_f = f_w'\left(s_f\right)\sigma_{ow}\sqrt{K/\phi}[J(s_{wr}) - \Delta J^*]dt \tag{48}$$

and integrate, using the condition that $x_f(t = 0) = 0$:

$$x_f^2\,\frac{1}{2}\left[\frac{1}{\lambda_T^*} - \frac{1}{\lambda_o(s_{wr})}\right] + x_f\,\frac{L}{\lambda_o(s_{wr})} + \left(-f_w'\left(s_f\right)\sigma_{ow}\sqrt{K/\phi}[J(s_{wr}) - \Delta J^*]t\right) = 0 \tag{49}$$

We introduce the critical time t_c when water reaches the outlet, defined by setting $x_f = L$ in (49), which results in:

$$t_c = \frac{\sqrt{\frac{\phi}{K}}L^2}{\sigma_{ow}}\,\frac{\frac{1}{2}\left[\frac{1}{\lambda_T^*} + \frac{1}{\lambda_o(s_{wr})}\right]}{f_w'\left(s_f\right)[J(s_{wr}) - \Delta J^*]}. \tag{50}$$

The solution for front position with time can then be expressed as:

$$\frac{x_f}{L} = \frac{1}{\frac{\lambda_o(s_{wr})}{\lambda_T^*} - 1}\left[-1 + \sqrt{1 + \left[\left(\frac{\lambda_o(s_{wr})}{\lambda_T^*}\right)^2 - 1\right]\frac{t}{t_c}}\right], \qquad (0 < t < t_c) \tag{51}$$

Average saturation is given by:

$$\bar{s}_w = \frac{1}{L}\int_{x=0}^{L} s_w dx = s_{wr} + \frac{x_f}{L}\left(s_f - s_{wr}\right)\frac{f_w\left(s_{eq}\right) - f_w(s_{wr})}{f_w\left(s_f\right) - f_w(s_{wr})}, \tag{52}$$

and recovery factor (of obtainable oil) is:

$$RF = \frac{\bar{s}_w - s_{wr}}{s_{eq} - s_{wr}}. \tag{53}$$

B. Late time solution

'Late time' means times after water has reached the outlet. The main assumption is that the imbibed water remains in the core and maintains a BL profile. The saturation at the outlet will be equal to s_f or higher: $s_w(x = L, t > t_c) \geq s_f$ hence the entire profile uses the continuous BL solution. The inlet water pressure is still zero, but the outlet condition of zero oil pressure now gives a water pressure that changes with the outlet water saturation s_{wR} and the outlet capillary pressure function:

$$p_{wL} = 0, \tag{54}$$

$$p_{wR} = -P_c\left(s_w(x = L, t)\right) = -P_c\left(s_{wR}(t)\right), \tag{55}$$

The saturation profile is described relative to the outlet water saturation by:

$$x(s_w) = L, \qquad (s_{wr} < s_w < s_{wR}), \tag{56}$$

$$x(s_w) = \frac{f'(s_w)}{f'(s_{wR})} L, \qquad (s_{wR} < s_w < s_{eq}), \tag{57}$$

We introduce scaling relative to the core length:

$$X = \frac{x}{L}, \qquad dX = \frac{dx}{L} \tag{58}$$

which gives the following imbibition rate expression:

$$u_T = -K\lambda_T(s_w)\frac{1}{L}\partial_X p_w - K\lambda_o(s_w)\frac{1}{L}\sigma_{ow}\sqrt{\frac{\phi}{K}}\partial_X J(s_w), \qquad (0 < \mathrm{X} < 1). \tag{59}$$

We find the pressure gradient:

$$\partial_X p_w = -\frac{Lu_T}{K\lambda_T} - (1 - f_w)\sigma_{ow}\sqrt{\phi/K}\,\partial_X J, \qquad (0 < X < 1), \tag{60}$$

which is integrated over the core to find the pressure drop:

$$p_{wR} - p_{wL} = -\frac{Lu_T}{K}\int_{X=0}^{1}\frac{1}{\lambda_T}dX - \sigma_{ow}\sqrt{\frac{\phi}{K}}\int_{X=0}^{1}(1 - f_w)\partial_X J dX. \tag{61}$$

Introducing a similar notation as before:

$$\frac{1}{\lambda_T^{**}(s_{wR})} = \int_{X=0}^{1}\frac{1}{\lambda_T}dX, \qquad \Delta J^{**}(s_{wR}) = \int_{X=0}^{1}(1 - f_w)\partial_X J dX \tag{62}$$

and applying boundary conditions (54) and (55) we obtain:

$$u_T = \frac{K}{L}\lambda_T^{**}(s_{wR})\sigma_{ow}\sqrt{\phi/K}\,[J(s_{wR}) - \Delta J^{**}(s_{wR})] \tag{63}$$

As indicated, the parameters λ_T^{**} and ΔJ^{**} are not constant, but depend on the current value of s_{wR}. The above equation gives the imbibition rate as a function of the saturation at the outlet. For a given saturation profile (given by s_{wR}) we obtain the average saturation as:

$$\begin{aligned}\bar{s}_w &= \frac{1}{L}\int_{x=0}^{L} s_w dx = s_{wr} + \frac{1}{L}\int_{s_w=s_{wr}}^{s_{wR}} L ds_w + \frac{1}{L}\int_{s_w=s_{wR}}^{s_{eq}}\frac{f'(s_w)}{f'(s_{wR})} L ds_w \\ &= s_{wR} + \frac{f(s_{eq}) - f(s_{wR})}{f'(s_{wR})}.\end{aligned} \tag{64}$$

Setting s_{wR} equal s_f or s_{eq}:

$$\bar{s}_w(s_{wR} = s_f) = s_f + \frac{f(s_{eq}) - f(s_f)}{f'(s_f)}, \qquad \bar{s}_w(s_{wR} = s_{eq}) = s_{eq}. \tag{65}$$

Verifies continuity with the early time solution, and uniform saturation corresponding to zero capillary pressure, respectively. The relation between average saturation and imbibition rate (when water enters at the inlet with flux $u_T f_w(s_{eq})$ and has zero flux at the outlet is found by integration of (13) as:

$$\phi\partial_t\bar{s}_w = \frac{\phi}{L}\int_{x=0}^{L}\partial_t s_w = \frac{1}{L}\int_{x=0}^{L} -u_T\partial_x f_w = \frac{u_T f_w(s_{eq})}{L}, \tag{66}$$

By combination of (63), (64) and (66) we obtain:

$$d_t\left(s_{wR} + \frac{f(s_{eq}) - f(s_{wR})}{f'(s_{wR})}\right) = \frac{Kf_w(s_{eq})}{\phi L^2}\lambda_T^{**}(s_{wR})\sigma_{ow}\sqrt{\phi/K}\,[J(s_{wR}) - \Delta J^{**}(s_{wR})], \tag{67}$$

which after integration with the condition $s_{wR}(t = t_c) = s_f$ yields:

$$t(s_{wR}) - t_c = \frac{L^2\sqrt{\frac{\phi}{K}}}{\sigma_{ow}}\frac{1}{f_w(s_{eq})}\int_{z=s_f}^{s_{wR}}\frac{\frac{d}{dy}\left(y + \frac{f(s_{eq}) - f(y)}{f'(y)}\right)_{y=z}}{\lambda_T^{**}(z)\,[J(z) - \Delta J^{**}(z)]}dz. \tag{68}$$

y, z are integration variables introduced to differ from the integration limit s_{wR}. This expression provides s_{wR} as an implicit function of time $t(s_{wR})$. With this relation determined we can apply (64) to calculate

average saturation at the times corresponding to the values of s_{wR}. Recovery follows from (53).

C. Special cases

The analytical solution has several special cases worth mentioning. Early time is assumed.

i. Special case I: Equal mobilities

If the effective total mobility behind the front equals the oil mobility ahead of the front ($\lambda_T^* = \lambda_o(s_{wr})$), (44) simplifies to:

$$x_f \frac{L}{\lambda_o(s_{wr})} + \left(-\frac{f_w'(s_f)K}{\phi} \sigma_{ow} \sqrt{\phi/K}\, [J(s_{wr}) - \Delta J^*]t \right) = 0, \tag{69}$$

which gives the following solution:

$$\frac{x_f}{L} = \frac{t}{t_c}, \qquad t_c = \frac{L^2 \sqrt{\frac{\phi}{K}}}{\sigma_{ow}} \frac{1}{f_w'(s_f)\lambda_o(s_{wr})[J(s_{wr}) - \Delta J^*]} \tag{70}$$

Average saturation and recovery are linearly related to front position, hence linear cumulative production with time is observed for such a situation although no assumption has been placed on whether the displacement is piston-like or not.

ii. Special case II: Piston-like displacement (PLD)

If the front saturation equals the highest imbibing saturation, i.e. $s_f = s_{eq}$, PLD occurs. That happens if s_{eq} is lower than the saturation where a tangent can be drawn on f_w starting from s_{wr} and can take place for mixed-wet media. The front is then determined by:

$$\frac{dx_f}{\mathrm{dt}} = \frac{1}{\phi} \frac{f_w(s_{eq}) - f_w(s_{wr})}{s_{eq} - s_{wr}} u_T = \frac{1}{\phi} \frac{\lambda_w(s_{eq})}{\lambda_T(s_{eq})} \frac{1}{s_{eq} - s_{wr}} u_T, \qquad (s_{wr} < s_w < s_{eq}). \tag{71}$$

According to (14) the total flux behind the front must equal the total flux ahead of the front:

$$u_T = -K\lambda_T(s_{eq}) \frac{p_{wf} - p_{wL}}{x_f - 0} = -K\lambda_o(s_{wr}) \frac{p_{oR} - p_{of}}{L - x_f}. \tag{72}$$

where $\lambda_T(s_{eq}) < \lambda_o(s_{wr})$ in line with PLD. Using that water and oil have zero pressure at the inlet and outlet, respectively, we obtain a relation between the front phase pressures:

$$p_{wf} = -\frac{\lambda_o(s_{wr})}{\lambda_T(s_{eq})} \frac{x_f}{L - x_f} p_{of}. \tag{73}$$

Introducing the constant front capillary pressure:

$$P_{cf} = p_{of} - p_{wf}, \tag{74}$$

we can solve (73) and (74) for p_{of}:

$$p_{of} = \frac{P_{cf}}{1 + \frac{\lambda_o(s_{wr})}{\lambda_T(s_{eq})} \frac{x_f}{L - x_f}}. \tag{75}$$

which inserted into (72) gives total flux as function of front position:

$$u_T = \frac{\sigma_{ow} \sqrt{\phi K} J_f}{\frac{L - x_f}{\lambda_o(s_{wr})} + \frac{x_f}{\lambda_T(s_{eq})}}. \tag{76}$$

From (71) and (76) we obtain a differential equation for the front position,

$$\frac{dx_f}{dt} = \frac{1}{\phi} \frac{\lambda_w(s_{eq})}{\lambda_T(s_{eq})} \frac{\sigma_{ow} \sqrt{\phi/K}}{s_{eq} - s_{wr}} \frac{KJ_f}{\frac{L - x_f}{\lambda_o(s_{wr})} + \frac{x_f}{\lambda_T(s_{eq})}}, \tag{77}$$

which is solved with the condition of $x_f(t = 0) = 0$:

(78) $$\frac{1}{2}x_f^2\left(\frac{1}{\lambda_T(s_{eq})}-\frac{1}{\lambda_o(s_{wr})}\right)+x_f\frac{L}{\lambda_o(s_{wr})}-\frac{1}{\phi}\frac{\lambda_w(s_{eq})}{\lambda_T(s_{eq})}\frac{K\sigma_{ow}\sqrt{\phi/K}J_f}{s_{eq}-s_{wr}}t=0.$$

The critical time t_c is then:

(79) $$t_c=\frac{L^2\sqrt{\frac{\phi}{K}}}{\sigma_{ow}}\frac{(s_{eq}-s_{wr})}{J_f(s_{wr})\lambda_w(s_{eq})}\ \frac{1+\frac{\lambda_T(s_{eq})}{\lambda_o(s_{wr})}}{2}.$$

and front position against time is expressed as:

(80) $$x_f=\frac{L}{\left(\frac{\lambda_o(s_{wr})}{\lambda_T(s_{eq})}-1\right)}\left(\sqrt{1+\left(\left(\frac{\lambda_o(s_{wr})}{\lambda_T(s_{eq})}\right)^2-1\right)\frac{t}{t_c}}-1\right),$$

Since $\frac{\lambda_o(s_{wr})}{\lambda_T(s_{eq})}>1$ we have $\frac{d^2x_f}{dt^2}<0$, i.e. decreasing imbibition rate. The average saturation is given by

(81) $$\bar{s}_w=\frac{1}{L}\int_{x=0}^{L}s_w dx=\frac{1}{L}\int_{x=0}^{x_f}s_{eq}dx+\frac{1}{L}\int_{x=x_f}^{L}s_{wr}dx=(s_{eq}-s_{wr})\frac{x_f}{L}+s_{wr}.$$

and recovery (from (53)) is given by:

(82) $$RF=\frac{x_f}{L}.$$

iii. Special case III: Infinite oil mobility

A special case of PLD is when the oil mobility is much higher than the water phase. This gives $\frac{\lambda_o(s_{wr})}{\lambda_T(s_{eq})}\approx\frac{\lambda_o(s_{wr})}{\lambda_o(s_{eq})}$ if MW media are assumed $(s_{eq}<1-s_{or})$ and same functional expressions of time scale and recovery as in (80) to (82), but the role of oil viscosity and oil relative permeability end point is eliminated. For SWW media $(s_{eq}=1-s_{or})$ we have $\frac{\lambda_o(s_{wr})}{\lambda_T(s_{eq})}\approx\frac{\lambda_o(s_{wr})}{\lambda_w(1-s_{or})}\gg 1$ resulting in:

(83) $$\frac{x_f}{L}=\sqrt{\frac{t}{t_c}},\qquad t_c=\frac{1}{2}\frac{L^2\sqrt{\frac{\phi}{K}}}{\sigma_{ow}}\frac{(s_{eq}-s_{wr})}{J_f(s_{wr})\lambda_w(s_{eq})}$$

where all effects of oil mobility are eliminated. Notably, square root of time recovery can be expected for SWW media at favorable mobility ratios, but not MW media (with more affinity to oil).

References

1. Al-Menhali, A., Niu, B., & Krevor, S. (2015). Capillarity and wetting of carbon dioxide and brine during drainage in Berea sandstone at reservoir conditions. *Water Resources Research*, *51*(10), 7895-7914.
2. Alvarez, J. O., & Schechter, D. S. (2017). Wettability alteration and spontaneous imbibition in unconventional liquid reservoirs by surfactant additives. *SPE Reservoir Evaluation & Engineering*, *20*(01), 107-117.
3. Amott, E. (1959). Observations relating to the wettability of porous rock. *Petroleum Transactions of AIME*, **216**, 156-162.
4. Andersen, P. Ø., Evje, S., & Hiorth, A. (2017a). Modeling of Spontaneous-Imbibition Experiments With Porous Disk—On the Validity of Exponential Prediction. *SPE Journal*, **22**(05), 1-326.
5. Andersen, P. Ø., Skjæveland, S. M., & Standnes, D. C. (2017b). A Novel Bounded Capillary Pressure Correlation with Application to Both Mixed and Strongly Wetted Porous Media. In *SPE Abu Dhabi International Petroleum Exhibition & Conference, Abu Dhabi, UAE*.
6. Andersen, P. Ø., Wang, W., Madland, M. V., Zimmermann, U., Korsnes, R. I., Bertolino, S. R. A., ... & Gilbricht, S. (2018). Comparative study of five outcrop chalks flooded at reservoir conditions:

chemo-mechanical behaviour and profiles of compositional alteration. *Transport in Porous Media*, **121**(1), 135-181.

7. Andersen, P. Ø., Brattekås, B., Nødland, O., Lohne, A., Føyen, T. L., & Fernø, M. A. (2019a). Darcy-Scale Simulation of Boundary-Condition Effects During Capillary-Dominated Flow in High-Permeability Systems. *SPE Reservoir Evaluation & Engineering,* **22**(02), 673-691.
8. Andersen, P. Ø., Lohne, A., Stavland, A., Hiorth, A., & Brattekås, B. (2019b). Core Scale Modeling of Polymer Gel Dehydration by Spontaneous Imbibition. *SPE Journal*, **24**(03), 1201-1219.
9. Andersen, P. Ø., Qiao, Y., Standnes, D. C., & Evje, S. (2019c). Cocurrent spontaneous imbibition in porous media with the dynamics of viscous coupling and capillary backpressure. *SPE Journal*, **24**(01), 158-177.
10. Andersen, P. Ø., Nesvik, E. K., & Standnes, D. C. (2020a). Analytical solutions for forced and spontaneous imbibition accounting for viscous coupling. *Journal of Petroleum Science and Engineering*.
11. Andersen, P. Ø., Walrond, K., Nainggolan, C. K., Pulido, E. Y., & Askarinezhad, R. (2020b). Simulation Interpretation of Capillary Pressure and Relative Permeability From Laboratory Waterflooding Experiments in Preferentially Oil-Wet Porous Media. *SPE Reservoir Evaluation & Engineering*, **23**(01), 230-246.
12. Anderson, W. G. (1987a). Wettability literature survey-part 4: Effects of wettability on capillary pressure. *Journal of petroleum technology*, *39*(10), 1-283.
13. Anderson, W. G. (1987b). Wettability literature survey part 5: the effects of wettability on relative permeability. *Journal of Petroleum Technology*, *39*(11), 1-453.
14. Bear, J. (2013). *Dynamics of fluids in porous media*. Courier Corporation.
15. Behbahani, H., & Blunt, M. J. (2005). Analysis of imbibition in mixed-wet rocks using pore-scale modeling. *Spe Journal*, *10*(04), 466-474.
16. Berg, S., & Ott, H. (2012). Stability of CO2–brine immiscible displacement. *International Journal of Greenhouse Gas Control*, *11*, 188-203.
17. Bourbiaux, B. J. (2009, January). Understanding the Oil Recovery Challenge of Water Drive Fractured Reservoirs. In *International Petroleum Technology Conference*.
18. Bourbiaux, B. J., & Kalaydjian, F. J. (1990). Experimental study of cocurrent and countercurrent flows in natural porous media. *SPE Reservoir Engineering*, **5**(03), 361-368.
19. Brooks, R. H., & Corey, A. T. (1966). Properties of porous media affecting fluid flow. *Journal of the Irrigation and Drainage Division*, **92**(2), 61-90.
20. Buckley, S. E., & Leverett, M. (1942). Mechanism of fluid displacement in sands. *Transactions of the AIME*, **146**(01), 107-116.
21. Chen, Z., Huan, G., & Ma, Y. (2006). Computational methods for multiphase flows in porous media (Vol. 2). SIAM.
22. Chiquet, P., Broseta, D., & Thibeau, S. (2007). Wettability alteration of caprock minerals by carbon dioxide. *Geofluids*, *7*(2), 112-122.
23. Deng, L., King, M.J. (2019) Theoretical investigation of two-ends-open free spontaneous imbibition. *Computational Geosciences,*
24. Dullien, F. A. (2012). *Porous media: fluid transport and pore structure*. Academic press.
25. Fathi, S. J., Austad, T., & Strand, S. (2011). Water-based enhanced oil recovery (EOR) by "smart water": Optimal ionic composition for EOR in carbonates. *Energy & fuels*, *25*(11), 5173-5179.
26. Fernø, M. A., Haugen, Å., Brattekås, B., Morrow, N. R. and Mason, G. (2015). Spontaneous Imbibition Revisited: A New Method to Determine Kr and Pc by Inclusion of the Capillary Backpressure. In *The 18th European Symposium on Improved Oil Recovery, EAGE, Dresden, Germany, 14-16 April*.
27. Hamidpour, E., Mirzaei-Paiaman, A., Masihi, M., & Harimi, B. (2015). Experimental study of some important factors on nonwetting phase recovery by cocurrent spontaneous imbibition. *Journal of Natural Gas Science and Engineering*, *27*, 1213-1228.

28. Hamon, G., & Vidal, J. (1986). Scaling-up the capillary imbibition process from laboratory experiments on homogeneous and heterogeneous samples. In *European Petroleum Conference*. Society of Petroleum Engineers.
29. Haugen, Å., M. A. Fernø, G. Mason and N. R. Morrow (2014) Capillary pressure and relative permeability estimated from a single spontaneous imbibition test. *Journal of Petroleum Science and Engineering* **115**, 66-77.
30. Haugen, Å., Fernø, M. A., Mason, G., & Morrow, N. R. (2015). The effect of viscosity on relative permeabilities derived from spontaneous imbibition tests. *Transport in Porous Media*, **106**(2), 383-404.
31. Karimi, M., Al-Maamari, R. S., Ayatollahi, S., & Mehranbod, N. (2016). Wettability alteration and oil recovery by spontaneous imbibition of low salinity brine into carbonates: Impact of Mg2+, SO42− and cationic surfactant. *Journal of Petroleum Science and Engineering*, *147*, 560-569.
32. Krevor, S., Blunt, M. J., Benson, S. M., Pentland, C. H., Reynolds, C., Al-Menhali, A., & Niu, B. (2015). Capillary trapping for geologic carbon dioxide storage–From pore scale physics to field scale implications. *International Journal of Greenhouse Gas Control*, *40*, 221-237.
33. Le Guen, S. S., & Kovscek, A. R. (2006). Nonequilibrium effects during spontaneous imbibition. *Transport in porous media*, *63*(1), 127-146.
34. Lenormand, R., Touboul, E., & Zarcone, C. (1988). Numerical models and experiments on immiscible displacements in porous media. *Journal of fluid mechanics*, *189*, 165-187.
35. Leverett, M. (1941). Capillary behavior in porous solids. *Transactions of the AIME*, *142*(01), 152-169.
36. Li, K. (2007). Scaling of spontaneous imbibition data with wettability included. *Journal of contaminant hydrology*, *89*(3-4), 218-230.
37. Li, K., & Horne, R. N. (2001). Characterization of Spontaneous Water Imbibition Into Gas-Saturated Rocks. *SPE Journal*, *6*(04), 375-384.
38. Li, K., & Horne, R. N. (2004). An analytical scaling method for spontaneous imbibition in gas/water/rock systems. *Spe Journal*, *9*(03), 322-329.
39. Li, Y., Ruth, D., Mason, G., & Morrow, N. R. (2006). Pressures acting in counter-current spontaneous imbibition. *Journal of Petroleum Science and Engineering*, **52**(1-4), 87-99.
40. Liu, H., Zhang, Y., & Valocchi, A. J. (2015). Lattice Boltzmann simulation of immiscible fluid displacement in porous media: Homogeneous versus heterogeneous pore network. *Physics of Fluids*, *27*(5), 052103.
41. Lohne, A. (2013). User's Manual for BugSim–an MEOR Simulator (V1. 2). Technical report, IRIS.
42. Ma, S., Morrow, N. R., & Zhang, X. (1997). Generalized scaling of spontaneous imbibition data for strongly water-wet systems. *Journal of Petroleum Science and Engineering*, **18**(3-4), 165-178.
43. Mattax, C. C., & Kyte, J. R. (1962). Imbibition oil recovery from fractured, water-drive reservoir. *SPE Journal*, **2**(02), 177-184.
44. Mason, G., & Morrow, N. R. (2013). Developments in spontaneous imbibition and possibilities for future work. *Journal of Petroleum Science and Engineering*, **110**, 268-293.
45. McPhee, C., Reed, J., & Zubizarreta, I. (2015). *Core analysis: a best practice guide*. Elsevier.
46. McWhorter, D. B., & Sunada, D. K. (1990). Exact integral solutions for two-phase flow. *Water Resources Research*, *26*(3), 399-413.
47. Meng, M., Ge, H., Ji, W., Shen, Y., & Su, S. (2015). Monitor the process of shale spontaneous imbibition in co-current and counter-current displacing gas by using low field nuclear magnetic resonance method. *Journal of Natural Gas Science and Engineering*, *27*, 336-345.
48. Meng, Q., Liu, H., Wang, J., & Zhang, H. (2016). Effect of wetting-phase viscosity on cocurrent spontaneous imbibition. *Energy & Fuels*, **30**(2), 835-843.
49. Meng, Q., Liu, H., & Wang, J. (2017). Effect of viscosity on oil production by cocurrent and countercurrent imbibition from cores with two ends open. *SPE Reservoir Evaluation & Engineering*, **20**(02), 251-259.

50. Meng, Q., Cai, Z., Cai, J., & Yang, F. (2019). Oil recovery by spontaneous imbibition from partially water-covered matrix blocks with different boundary conditions. *Journal of Petroleum Science and Engineering*, *172*, 454-464.
51. Nygård, J. I., & Andersen, P. Ø. (2020). Simulation of Immiscible Water-Alternating-Gas Injection in a Stratified Reservoir: Performance Characterization Using a New Dimensionless Number. *SPE Journal*.
52. Pickell, J. J., Swanson, B. F., & Hickman, W. B. (1966). Application of air-mercury and oil-air capillary pressure data in the study of pore structure and fluid distribution. *Society of Petroleum Engineers Journal*, *6*(01), 55-61.
53. Pooladi-Darvish, M., & Firoozabadi, A. (2000). Cocurrent and countercurrent imbibition in a water-wet matrix block. *SPE Journal*, **5**(01), 3-11.
54. Reed, J., & Maas, J. (2018, August). Review of the intercept method for relative permeability correction using a variety of case study data. In *The International Symposium of the Society of Core Analysts, Trondheim, Norway*.
55. Roychaudhuri, B., Xu, J., Tsotsis, T. T., & Jessen, K. (2014, April). Forced and spontaneous imbibition experiments for quantifying surfactant efficiency in tight shales. In *SPE Western North American and Rocky Mountain Joint Meeting*. Society of Petroleum Engineers.
56. Shen, Y., Ge, H., Li, C., Yang, X., Ren, K., Yang, Z., & Su, S. (2016). Water imbibition of shale and its potential influence on shale gas recovery—a comparative study of marine and continental shale formations. *Journal of Natural Gas Science and Engineering*, *35*, 1121-1128.
57. Standnes, D. C. (2004). Experimental study of the impact of boundary conditions on oil recovery by co-current and counter-current spontaneous imbibition. *Energy & fuels*, **18**(1), 271-282.
58. Schmid, K. S., Geiger, S., & Sorbie, K. S. (2011). Semianalytical solutions for cocurrent and countercurrent imbibition and dispersion of solutes in immiscible two-phase flow. *Water Resources Research*, **47**(2).
59. Silin, D., & Patzek, T. (2004). On Barenblatt's model of spontaneous countercurrent imbibition. *Transport in porous media*, *54*(3), 297-322.
60. Standnes, D. C., Evje, S., & Andersen, P. Ø. (2017). A novel relative permeability model based on mixture theory approach accounting for solid–fluid and fluid–fluid interactions. *Transport in Porous Media*, **119**(3), 707-738.
61. Standnes, D. C., & Andersen, P. Ø. (2017). Analysis of the impact of fluid viscosities on the rate of countercurrent spontaneous imbibition. *Energy & fuels*, **31**(7), 6928-6940.
62. Terez, I. E., & Firoozabadi, A. (1999). Water injection in water-wet fractured porous media: Experiments and a new model with modified Buckley-Leverett theory. *SPE Journal*, *4*(02), 134-141.
63. Unsal, E., Mason, G., Morrow, N. R., & Ruth, D. W. (2007). Co-current and counter-current imbibition in independent tubes of non-axisymmetric geometry. *Journal of colloid and interface science*, **306**(1), 105-117.
64. Vavra, C. L., Kaldi, J. G., & Sneider, R. M. (1992). Geological applications of capillary pressure: a review (1). *AAPG bulletin*, *76*(6), 840-850.
65. Wang, M., Abeykoon, G. A., Argüelles-Vivas, F. J., & Okuno, R. (2019). Ketone solvent as a wettability modifier for improved oil recovery from oil-wet porous media. *Fuel*, *258*, 116195.
66. Wang, X., & Sheng, J. J. (2018). A self-similar analytical solution of spontaneous and forced imbibition in porous media. *Advances in Geo-Energy Research*, **2**(3), 260-268.
67. Wang, Y., Aryana, S. A., Furtado, F., & Ginting, V. (2018). Analysis of nonequilibrium effects and flow instability in immiscible two-phase flow in porous media. *Advances in Water Resources*, *122*, 291-303.
68. Washburn, E. W. (1921). The dynamics of capillary flow. *Physical review*, *17*(3), 273.
69. Xie, X. and Morrow, N. R. (2001). Oil Recovery By Spontaneous Imbibition From Weakly Water-Wet Rocks. *Petrophysics,* **42**(4).
70. Yortsos, Y. C., & Fokas, A. S. (1983). An analytical solution for linear waterflood including the effects of capillary pressure. *SPE Journal*, **23**(01), 115-124.

71. Zeppieri, S., Rodríguez, J., & López de Ramos, A. L. (2001). Interfacial tension of alkane+ water systems. *Journal of Chemical & Engineering Data*, **46**(5), 1086-1088.
72. Zhang, D. L., Liu, S., Puerto, M., Miller, C. A., & Hirasaki, G. J. (2006). Wettability alteration and spontaneous imbibition in oil-wet carbonate formations. *Journal of Petroleum Science and Engineering*, *52*(1-4), 213-226.
73. Zhang, C., Oostrom, M., Wietsma, T. W., Grate, J. W., & Warner, M. G. (2011). Influence of viscous and capillary forces on immiscible fluid displacement: Pore-scale experimental study in a water-wet micromodel demonstrating viscous and capillary fingering. *Energy & Fuels*, *25*(8), 3493-3505.
74. Zhou, Z., Abass, H., Li, X., Bearinger, D., & Frank, W. (2016). Mechanisms of imbibition during hydraulic fracturing in shale formations. *Journal of Petroleum Science and Engineering*, *141*, 125-132.